Activated PTKs and PI(3)K in resting XLA neutrophils

Assembly and activation of the cytosolic components and Rac requires the involvement of kinases such as PTKs, PI(3)K and protein kinase C. We thus explored a potential signaling pathway that would lead to the partial assembly of NADPH oxidase. First, we examined the extent of tyrosine phosphorylation of cellular substrates in Btk-deficient and Btk-sufficient neutrophils before and after stimulation with PMA. Btk-deficient neutrophils showed hyperphosphorylation of protein species in the range of 50–53 kilodaltons (kDa), 72 kDa, 85 kDa and 150 kDa at baseline relative to phosphorylation in neutrophils from healthy controls (**Fig. 5a**). TLR4-mediated stimulation led to more phosphorylation of protein species 38 kDa, 50–53 kDa, 60 kDa, 72 kDa and 85 kDa in size in Btk-deficient neutrophils (**Supplementary Fig. 4a**).

In contrast, the baseline PTK activity in monocytes from patients with XLA was unaltered or slightly diminished relative to that of monocytes from healthy controls. TLR2-stimulated activation of PTKs was largely similar or slightly less in the absence of Btk (**Supplementary Fig. 4b**). We were able to directly ascribe the enhanced PTK activity to the absence of Btk, as transduction of recombinant Btk into neutrophils from patients with XLA restored baseline phosphorylation to that seen in neutrophils from healthy controls (**Fig. 5b**).

We next searched for tyrosine-phosphorylated proteins in Btk-deficient neutrophils through the use of phosphorylation-specific antibodies. The expression and activation of Tec and Bmx, TFKs present in neutrophils, was not upregulated in neutrophils from patients with XLA (**Fig. 5c**), which indicated that they did not compensate for Btk function. However, we found that the tyrosine-phosphorylated proteins 50–53 kDa, 72 kDa, 85 kDa and 150 kDa in size were the kinases Lyn and c-Src, Syk, the p85 subunit of PI(3)K (class IA) and FAK, respectively (**Fig. 5d,e**). We found that c-Src, Syk, PI(3)K-p85 and FAK were phosphorylated at their tyrosine residues that have a positive regulatory function. Notably, Lyn, a kinase known to have positive as well as negative roles in the modulation of myeloid function, was phosphorylated at Tyr507, a negative regulatory site[29–31].

We first focused on PI(3)K, as PI(3)K activation targets Rac2 to flavocytochrome b_{558}; this process is important for converting

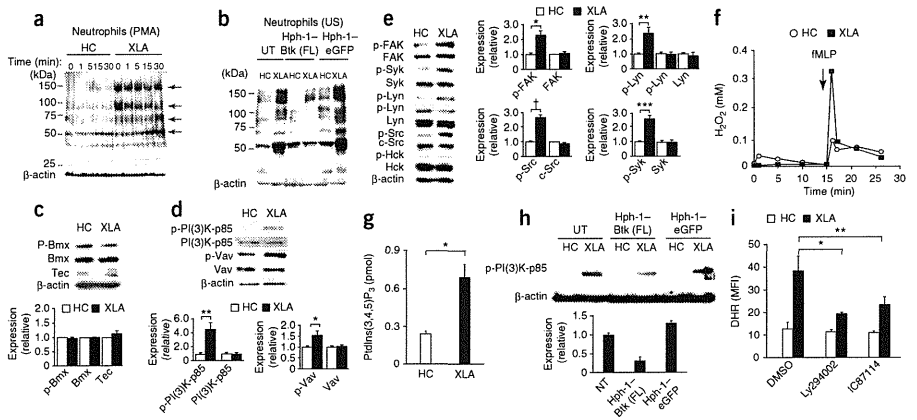

Figure 5 Btk-deficient neutrophils have higher baseline activity of PTKs and PI(3)K, which is reversed by transduction of recombinant Btk protein. (**a**) Immunoblot analysis of phosphorylated tyrosine in lysates of PMA-stimulated neutrophils from healthy controls ($n = 5$) and patients with XLA ($n = 7$). Arrows indicate hyperphosphorylated proteins in neutrophils from patients with XLA at 0 min. (**b**) Immunoblot analysis of phosphorylated tyrosine (as in **a**) in lysates from unstimulated (US) neutrophils from healthy controls ($n = 4$) and patients with XLA ($n = 5$), left untransduced or transduced with Hph-1–tagged full-length Btk or eGFP. (**c**,**d**) Immunoblot analysis (top) of whole-cell lysates of neutrophils from healthy controls ($n = 5$) and patients with XLA ($n = 7$), probed for total and phosphorylated Bmx and total Tec (**c**) or total and phosphorylated PI(3)K-p85 and Vav (phosphorylated at Tyr508 (PI(3)K-p85) or Tyr174 (Vav); **d**). Phosphorylated Tec was not detected by immunoblot analysis of phosphorylated tyrosine in samples immunoprecipitated with anti-Tec (data not shown). Bottom, quantification of the expression at top, presented relative to expression of β-actin in neutrophils from healthy controls, set as 1. $*P = 0.038$ and $**P = 0.0001$ (Student's *t*-test). (**e**) Immunoblot analysis (left) of neutrophils from healthy controls ($n = 5$) and patients with XLA ($n = 7$), probed for total PTKs and PTKs phosphorylated at Tyr576 and Tyr577 (FAK); Tyr524 and Tyr525 (Syk); Tyr507 (Lyn; top) or Tyr397 (Lyn; bottom); (Tyr416 (c-Src); and Tyr411 (the kinase Hck). Phosphorylated PTKs Fgr and Yes were undetectable (data not shown). Right, quantification as in **c**,**d**. $*P = 0.033$, $**P = 0.004$, $***P = 0.0007$ and $\dagger P = 0.0002$ (Student's *t*-test). (**f**) H_2O_2 production by fMLP-stimulated neutrophils from healthy controls and patients with XLA ($n = 5$ per group). (**g**) Enzyme-linked immunosorbent assay of phosphatidylinositol-(3,4,5)-trisphosphate ($PtdIns(3,4,5)P_3$) in unstimulated neutrophils from patients with XLA ($n = 5$). $*P = 0.0005$ (Student's *t*-test). (**h**) Immunoblot analysis (top) of phosphorylated PI(3)K-p85 in neutrophils from healthy controls and patients with XLA ($n = 5$ per group), left untransduced or transduced with Hph-1–tagged full-length Btk or eGFP. Detection of phosphorylated PI(3)K-p85 in neutrophils from healthy controls required longer exposure. Below, quantification of results above, presented relative to the expression of phosphorylated PI(3)K-p85 relative to that of β-actin in neutrophils from patients with XLA, set as 1. (**i**) Production of ROS in neutrophils from patients with XLA, treated with dimethyl sulfoxide (DMSO) or preincubated with Ly294002 (universal PI(3)K inhibitor; 50 μM)[32] or IC87114 (PI(3)Kδ inhibitor; 1 μM (a concentration that does not inhibit PI(3)Kα, PI(3)Kβ or PI(3)Kγ)[33]) and stimulated with fMLP. $*P = 0.006$ and $**P = 0.003$ (Student's *t*-test). Data are representative of or pooled from six (**a**,**f**), seven (**b**–**e**), four (**g**), eight (**h**) or five (**i**) independent experiments (mean and s.d. in **c**–**e**,**g**–**i**).

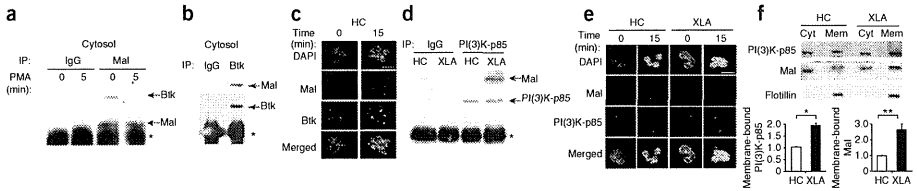

Figure 6 Mal in neutrophils from healthy controls associates with Btk in the resting state and translocates to the plasma membrane after stimulation, whereas Mal associates with PI(3)K at the plasma membrane in Btk-deficient neutrophils. (**a**,**b**) Coimmunoprecipitation analysis of Btk and Mal in the cytoplasmic fraction of neutrophils from healthy controls, left unstimulated (0 (**a**), b) or stimulated for 5 min with PMA (5 (**a**)). IP, immunoprecipitation; IgG, control antibody. *, immunoglobulin light chain (**a**) or heavy chain (**b**). (**c**) Confocal microscopy of neutrophils from healthy controls, left unstimulated (0) or stimulated for 15 min with PMA (15), then stained with anti-Mal (red) and anti-Btk (green) and counterstained with DAPI. Original magnification, ×600; scale bar, 10 μm. (**d**) Coprecipitation analysis of PI(3)K-p85 and Mal in membrane fraction of neutrophils from healthy controls and patients with XLA. *, immunoglobulin heavy chain. (**e**) Confocal microscopy of neutrophils from healthy controls and patients with XLA, left unstimulated or stimulated for 15 min with PMA, then stained with anti-Mal (red) and anti-PI(3)K-p85 (green) and counterstained with DAPI. Scale bar, 10 μm. (**f**) Immunoblot analysis (above) of PI(3)K-p85 and Mal in the cytoplasm and plasma membrane of unstimulated neutrophils from healthy controls and patients with XLA. Below, quantification of results above, presented relative to the expression of flotillin in neutrophils from healthy controls, set as 1. $*P = 0.0035$ and $**P = 0.0021$ (Student's *t*-test). Data are representative of three (**a**,**b**), four (**c**,**e**), six (**d**) or seven (**f**) independent experiments (mean and s.d. in **f**).

neutrophils into a 'primed' state in which they are ready for complete activation of NADPH oxidase triggered by stimuli such as fMLP. Indeed, Btk-deficient neutrophils were in a primed state, as fMLP alone elicited excessive production of ROS (**Fig. 5f**). Greater phosphorylation of PI(3)K-p85 was accompanied by more enzymatic activity, as shown by more baseline production of phosphatidylinositol-(3,4,5)-trisphosphate and by phosphorylation of the adaptor Vav (**Fig. 5d**,**g**). Furthermore, augmented PI(3)K activation was normalized, although only partially, by transduction of full-length Btk linked to Hph-1 (**Fig. 5h**).

The importance of PI(3)K in inducing the primed state was supported by data showing inhibition of fMLP-driven production of ROS by preincubation of Btk-deficient neutrophils with the universal PI(3)K inhibitor LY294002 at a concentration of 50 μM (refs. 32,33). We observed this inhibition in cells incubated with the PI(3)Kδ-specific inhibitor IC87114 at a concentration of 1 μM (ref. 33) but not in those incubated with the PI(3)Kγ-specific inhibitor AS605240 at a concentration of 8 nM (ref. 34; **Fig. 5i** and **Supplementary Fig. 5a**). These findings suggested PI(3)Kδ activation was involved in the excessive ROS response.

Interaction of membrane-targeted Mal with PI(3)K

We next sought the reason for the PI(3)K activation in the absence of Btk. For this, we first focused on a molecule that interacts with both Btk and PI(3)K. Evidence obtained with monocytes indicates that Mal is a critical component of TLR2-TLR4 signaling and is a target of Btk[13,14,20,21]. The TLR signal triggers activation of Btk, which in turn phosphorylates Mal. Phosphorylated Mal translocates to the plasma membrane via phosphatidylinositol-(4,5)-bisphosphate ($PtdIns(4,5)P_2$) and then interacts with and activates PI(3)K[35].

Unexpectedly, coimmunoprecipitation assays of neutrophils from human controls demonstrated that Mal was associated with Btk in the resting state (**Fig. 6a**,**b**). We observed colocalization of Mal and Btk in the cytoplasm and, after activation of cells with PMA, we detected the Mal-Btk complex at the membrane by immunofluorescence staining (**Fig. 6c**).

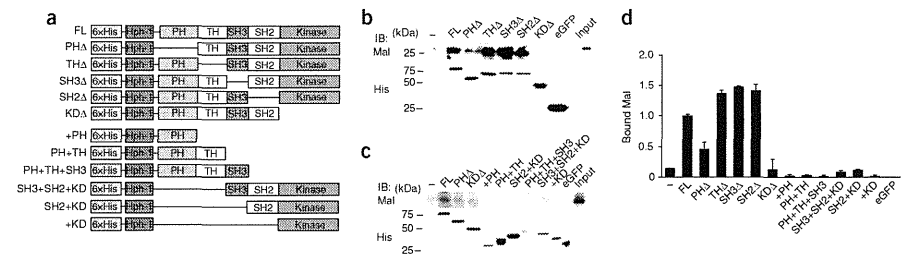

Figure 7 Btk associates with Mal at the PH and kinase domains. (**a**) Hph-1–tagged Btk constructs: full-length Btk (FL); Btk mutants with deletion of the PH domain (PHΔ), Tec homology (THΔ), SH3 domain (SH3Δ), SH2 domain (SH2Δ) or kinase domain (KDΔ); and Btk mutants with truncation retaining (+) only some domains (bottom six). (**b**,**c**) Immunoblot analysis (IB) of Mal (top) in extracts of cytoplasm of neutrophils from healthy controls, incubated with nickel beads bound to Hph-1–tagged recombinant full-length Btk or the deletion mutants (**b**) or truncation mutants (**c**) in **a**, or to Hph-1–tagged eGFP (negative control). Below, immunoblot analysis after rebinding to nickel beads, probed with anti-histidine (His). To make these as equimolar as possible, more beads were added for the +PH, PH+TH+SH3, SH3+SH2+KD and +KD constructs. Input, cytoplasmic extracts without precipitation. (**d**) Quantification of Mal bound to the recombinant Btk proteins based on the results in **b**,**c** ($n = 4$ donors), presented to results for full-length Btk, set as 1. Data are representative of four experiments (**b**,**c**) or are a summary of four independent experiments (**d**; mean and s.d.).

We did not detect the association of Mal with PI(3)K-p85 in unstimulated neutrophils from healthy controls; however, we did observe this association in Btk-deficient neutrophils before stimulation with PMA (**Fig. 6d**). Moreover, confocal fluorescence microscopy showed targeting of the PI(3)K-p85–Mal complex to the membrane in the absence of Btk, whereas we observed the complex at the membrane after stimulation with PMA in the presence of Btk (**Fig. 6e**). In addition, most of the PI(3)K-p85 and Mal was present in the membrane fraction in neutrophils from patients with XLA (**Fig. 6f**). These data suggested that Btk in resting neutrophils was involved in confining Mal to the cytoplasm.

The mode of the Btk-Mal association

Btk phosphorylates Mal at Tyr86, Tyr106 and Tyr187, and the Btk-Mal interaction requires Pro125, Tyr86, Tyr106 and Tyr159 in Mal, whereas the critical site in Btk for this association remains unknown[21,22]. To clarify the region of Btk required for the cytoplasmic Btk-Mal association, we generated various Btk deletion mutants fused to histidine-tagged Hph-1 (**Fig. 7a**) and assessed their binding to Mal (**Fig. 7**). We incubated nickel bead–bound recombinant proteins with the cytoplasmic fraction of control neutrophils and evaluated the associations by immunoblot analysis with anti-Mal. Full-length Btk effectively bound to cytoplasmic Mal prepared from control neutrophils, but a control fusion of histidine-tagged Hph-1 and enhanced green fluorescent protein (eGFP) did not. Btk with deletion of the kinase domain almost completely lost the ability to interact with Mal, and Btk with deletion of the PH domain showed less binding to Mal. In contrast, recombinant proteins lacking the Tec homology domain, the Src homology 3 domain or the Src homology 2 domain had slightly greater capacity to associate with Mal (**Fig. 7b,d**). Other truncated Btk recombinant proteins without either the PH domain or kinase domain failed to bind to Mal (**Fig. 7c,d**), which suggested that both the PH domain and kinase domain are critical for the Btk-Mal interaction.

PTKs associate with Mal and regulate PI(3)K activation

The precise mechanism of PI(3)K activation triggered by membrane-associated Mal is largely unknown. As several PTKs were phosphorylated

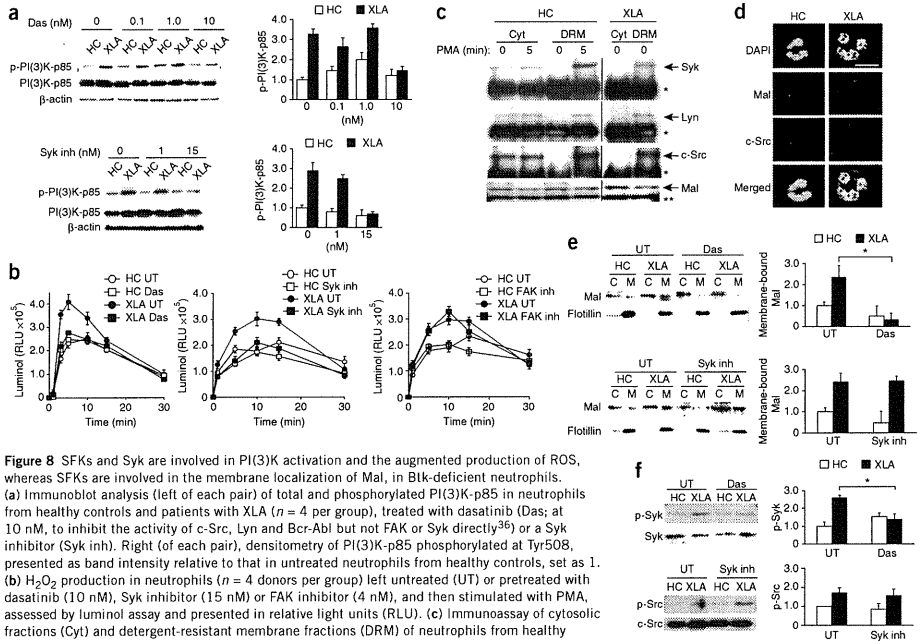

Figure 8 SFKs and Syk are involved in PI(3)K activation and the augmented production of ROS, whereas SFKs are involved in the membrane localization of Mal, in Btk-deficient neutrophils. (**a**) Immunoblot analysis (left of each pair) of total and phosphorylated PI(3)K-p85 in neutrophils from healthy controls and patients with XLA ($n = 4$ per group), treated with dasatinib (Das; at 10 nM, to inhibit the activity of c-Src, Lyn and Bcr-Abl but not FAK or Syk directly[36]) or a Syk inhibitor (Syk inh). Right (of each pair), densitometry of PI(3)K-p85 phosphorylated at Tyr508, presented as band intensity relative to that in untreated neutrophils from healthy controls, set as 1. (**b**) H_2O_2 production in neutrophils ($n = 4$ donors per group) left untreated (UT) or pretreated with dasatinib (10 nM), Syk inhibitor (15 nM) or FAK inhibitor (4 nM), and then stimulated with PMA, assessed by luminol assay and presented in relative light units (RLU). (**c**) Immunoassay of cytosolic fractions (Cyt) and detergent-resistant membrane fractions (DRM) of neutrophils from healthy controls and patients with XLA, left untreated (0) or treated for 5 min with PMA (5), followed by immunoprecipitation with anti-Mal and immunoblot analysis with anti-Syk, anti-Lyn, anti-c-Src or anti-Mal. *, immunoglobulin heavy chain; **, immunoglobulin light chain. (**d**) Confocal microscopy of neutrophils from healthy controls and patients with XLA ($n = 3$ per group), stained with anti-Mal (red) and anti-c-Src (blue) and counterstained with DAPI. Original magnification, ×600; scale bar, 10 μm. (**e**) Immunoblot analysis (left) of Mal in the cytoplasm (C) and membrane (M) of neutrophils from healthy controls and patients with XLA ($n = 5$ per group), left untreated or treated as in **a**. Right, quantification of results for Mal (left), presented relative to that of flotillin in the membrane fraction of neutrophils from healthy controls, set as 1. *$P = 0.0024$ (Student's *t*-test). (**f**) Immunoblot analysis of total Syk and Syk phosphorylated at Tyr524 and Tyr525 (top left) and of total c-Src and c-Src phosphorylated at Tyr416 (bottom left) in neutrophils from healthy controls and patients with XLA, left untreated or treated with dasatinib (top left) or Syk inhibitor (bottom left). Right, quantification of band intensity relative to that of β-actin in untreated neutrophils from healthy controls, set as 1. *$P = 0.013$ (Student's *t*-test). Data are from four (**a**) or five (**f**) independent experiments, are from one representative of four independent experiments (**c**) or are representative of four experiments (**b**,**e**) or three experiments (**c**; mean and s.d. in **a**,**b**,**e**,**f**).

in resting neutrophils from patients with XLA, we first used PTK inhibitors to investigate whether PTKs were involved in the PI(3)K activation. Inhibition of the activity of Src-family kinases (SFKs) by dasatinib (at a concentration of 10 nM)[36] led to normalized phosphorylation of PI(3)K-p85 in neutrophils derived from patients with XLA. Similarly, a Syk inhibitor (at a concentration of 15 nM)[37] but not a FAK inhibitor (at a concentration of 10 nM)[38] abrogated the hyperphosphorylation of PI(3)K (**Fig. 8a** and data not shown). The lower PI(3)K phosphorylation produced by dasatinib or the Syk inhibitor was accompanied by normalized production of ROS (**Fig. 8b**), which indicated that SFKs and Syk were involved in the augmented production of ROS in neutrophils from patients with XLA.

The findings noted above prompted us to determine whether the activated PTKs associated with Mal. SFKs are recruited to lipid rafts when activated for the assembly of signal components[39,40]. Coprecipitation assays showed that Lyn, c-Src and Syk interacted with Mal at the rafts of Btk-deficient neutrophils before stimulation (**Fig. 8c**). We also observed the colocalization of Mal and c-Src at the membrane by confocal fluorescence microscopy (**Fig. 8d**). We observed the interaction at the rafts of control neutrophils only after stimulation with PMA (**Fig. 8c** and **Supplementary Fig. 6**).

SFKs are cytoplasmic kinases and are anchored to the plasma membrane through myristoylation and palmitoylation[39,40]. Coprecipitation assays showed that Lyn, c-Src and Syk were associated with Mal in the cytosol of neutrophils from healthy controls but not in Btk-deficient neutrophils (**Fig. 8c**). We also confirmed by immunofluorescence staining the presence of c-Src associated with Mal in the cytoplasm but not in the membrane of normal resting neutrophils (**Fig. 8d**).

We next studied whether the membrane localization of Mal was regulated by SFKs or by Syk. The localization of Mal to the membrane in Btk-deficient neutrophils was diminished to normal amounts in cells treated with dasatinib but not those treated with the Syk inhibitor (**Fig. 8e**), which suggested that kinase activity of SFKs was required for membrane recruitment or maintenance of membrane-anchoring of Mal. Treatment of neutrophils from patients with XLA with dasatinib resulted in less baseline Syk phosphorylation, whereas incubation with the Syk inhibitor did not abrogate the hyperphosphorylation of c-Src (**Fig. 8f**), which indicated that Syk was downstream of SFKs in the steady-state signaling cascade of Btk-deficient neutrophils.

Collectively, the data reported above indicated that at least some PTKs associated with Mal together with Btk in the cytoplasm; in the absence of Btk, SFKs and Mal translocated to the membrane. The membrane-recruited PTKs formed a complex with and phosphorylated PI(3)K-p85 (**Supplementary Fig. 7**). It is still unclear which neutrophil SFK contributes to PI(3)K activation. Our findings may indicate that c-Src (or other SFKs) but not Lyn is (are) directly involved in the PI(3)K activation in Btk-deficient neutrophils; however, the possibility of an indirect contribution of Lyn to the phosphorylation of PI(3)K-p85 cannot be excluded solely by the inhibitor assay.

DISCUSSION

So far, most data have posited Btk as an essential molecule in innate immune responses[12–15,23,25]. Here we have shown that Btk is a negative regulator of signal transduction that leads to activation of NADPH oxidase and a molecule that prevents excessive neutrophil responses. Neutropenia in patients with XLA is usually induced by infection and is observed less often after immunoglobulin supplementation. This phenomenon can most probably be explained by ROS-mediated apoptosis of neutrophils triggered by the engagement of innate receptors and not by abnormal myeloid differentiation.

Our study suggested that Btk serves as a cytosolic component that interacts with Mal to prevent its translocation to the membrane and its interactions with PI(3)K until the appropriate stimulation is received. Both the PH and kinase domains of Btk were necessary for association with cytoplasmic Mal and were important for proper and coordinated initiation of the TLR and TNF receptor responses in human neutrophils. A similar mode of interaction has been demonstrated for the association of Btk with the cell-surface death receptor Fas (CD95) in B cells. Btk associates with Fas via its PH and kinase domains and prevents the interaction of Fas with the Fas-associated death domain and thus serves as a negative regulator of the Fas death-inducing signaling complex[41]. Notably, Btk serves as a negative regulator of apoptosis in both signaling systems.

SFKs were also involved in the baseline activation of PI(3)K in Btk-deficient neutrophils. We detected the association of c-Src, Lyn and Syk with Mal in the membrane raft in the absence of Btk. In addition, localization of Mal to the membrane in Btk-defective neutrophils was dependent on SFKs. These findings may indicate that SFKs serve as a substitute for the function of Btk in guiding the localization of Mal, albeit in an unregulated way. In neutrophils from control subjects, SFKs and Mal were associated in the cytoplasm and localized to the raft after stimulation. The mode of the SFK-Mal interaction remains unclear; however, we speculate that the kinase domain is involved, as SFKs lack a PH domain and the kinase domains of SFKs and Btk share 40–45% homology. Precise mapping of the Mal-binding site in the Btk kinase domain would help to clarify the SFK-Mal association site. Notably, neutrophils had more abundant expression of Mal than did monocytes (data not shown). Our data suggest that Mal is a critical coordinator of the priming signal and that its localization is tightly controlled by Btk.

Limited data indicate a role for PTKs in the production of ROS in neutrophils, particularly in humans. Lyn is reported to be a signaling component of the immunoglobulin receptors FcγRI and FcγRII or the receptor for the hematopoietic cytokine G-CSF, as well as an activator of PI(3)K[30,42], but is also noted for its ability to negatively regulate myeloid-cell signaling through phosphorylation of inhibitory receptors and recruitment of phosphatases[29]. Lyn-deficient neutrophils produce less ROS than Lyn-sufficient neutrophils do after stimulation with G-CSF[30] but show an enhanced respiratory burst after integrin-mediated signaling[29,31]. ROS responses triggered by *Aspergillus* species are totally dependent on Syk in mouse neutrophils[43]. The phosphorylation at different regulatory sites in Lyn versus c-Src in Btk-deficient neutrophils is notable. However, overall, PTKs in unstimulated neutrophils from patients with XLA seem to function as positive signal regulators. These data, along with our observations, suggest a potential contribution of SFKs and Syk to the early phase of NADPH oxidase activation in human neutrophils.

Activation of TFKs occurs downstream of SFKs in signaling pathways[40]. However, in neutrophils, Btk regulates baseline SFK activation. There are several possible mechanisms to explain how defective Btk is connected to SFK activation. We first speculated that Btk controls SFKs through the activation of negative SFK regulators. We investigated the Src kinase Csk and its regulatory molecule Cbp[44], but found no difference in the expression, localization or phosphorylation of Csk or Cbp (data not shown). As a second possible mechanism, SFKs but not TFKs may have been activated to compensate for Btk function in neutrophils. It is noteworthy that Btk regulates PtdIns(4,5)P_2 synthesis, acting as a shuttle to bring type I phosphatidylinositol-4-phosphate 5-kinases to the plasma membrane in B cells[45]. Although the role of Btk in PtdIns(4,5)P_2 production in human neutrophils has not been addressed, the generation of PtdIns(4,5)P_2 is a critical

step in the activation of NADPH oxidase. SFKs may have directly or indirectly served as a substitute for the function of Btk in neutrophils from patients with XLA. Finally, the cytoplasmic association of SFKs with Mal but without Btk may have resulted in SFK activation and Lyn inhibition. The phosphorylation of SFKs and subsequent modification of Mal by SFKs may have led to the translocation of Mal in the absence of Btk.

Neutrophils from patients with XLA show excessive production of ROS, but neutrophils from mice with X-linked immunodeficiency show poor ROS induction[15]. One possibility that could explain this discrepancy is the difference between mice and humans in the involvement of Btk in the NADPH oxidase pathway. Another possibility is the difference in the contributions of various members of the PI(3)K family to neutrophil activation. The primed production of ROS requires sequential activation of PI(3)Kγ and PI(3)Kδ in humans, whereas the production of ROS is largely dependent on PI(3)Kγ alone in mice[16]. A third possibility is differences in the methods of neutrophil collection from mice and in our study. Neutrophils collected from the peritoneum after treatment with thioglycolate broth may have been stimulated by that treatment[15]. The production of ROS was not augmented or compromised in neutrophils from patients with XLA in one study[26]. That may also have resulted from a relatively harsh isolation technique of hypotonic shock or from non–endotoxin-free conditions (for example, lipopolysaccharide in FBS) at any point of the experiment.

In this study, we have reported that Btk serves as a critical gatekeeper of neutrophil response. Our study suggests that the regulation of neutrophil activation and apoptosis in various human diseases could be achieved by manipulation of Btk. Future studies should explore the role of Btk in controlling the production of ROS and apoptosis of basophils, mast cells and eosinophils. Finally, ROS-mediated induction of apoptosis after suboptimal or optimal stimuli may be worth investigating in immature and precursor cells of the immune reponse to determine the role of Btk in their survival, proliferation and differentiation.

METHODS

Methods and any associated references are available in the online version of the paper at http://www.nature.com/natureimmunology/.

Note: Supplementary information is available on the Nature Immunology website.

ACKNOWLEDGMENTS

We thank E. Tsitsikov, E. Rachlin, K. Imai and J. Yata for discussions; all patients who participated in this study; S. Goo Rhee (Ewha Womans University) for antibody to Prx1 phosphorylated at Tyr194; and J.A. Lindquist (Otto-von-Guericke University) for antibody to Cbp (PAG) phosphorylated at Tyr317. Supported by the Ministry of Health, Labour and Welfare of Japan (H. Kane, S.N. and T.M.), the Ministry of Education, Culture, Sports, Science and Technology of Japan (S.M. and T.M.) and by the National Research Foundation of Korea (National Creative Research Initiatives grant to S.-K.L.).

AUTHOR CONTRIBUTIONS

F.H. did experiments; E.-S.K. and S.-K.L. contributed to protein-delivery experiments and provided some technical support; H. Kano and H. Kane made suggestions on data analysis and interpretation; S.N. and S.M. provided advice on project planning and data interpretation; M.T. provided advice on project plan and edited the manuscript; T.M. directed the project, designed research and wrote the manuscript; and all authors reviewed and approved the manuscript.

COMPETING FINANCIAL INTERESTS

The authors declare no competing financial interests.

Published online at http://www.nature.com/natureimmunology/.
Reprints and permissions information is available online at http://www.nature.com/reprints/index.html.

1. Flannagan, R.S., Cosio, G. & Grinstein, S. Antimicrobial mechanisms of phagocytes and bacterial evasion strategies. *Nat. Rev. Microbiol.* **7**, 355–366 (2009).
2. Nauseef, W.M. How human neutrophils kill and degrade microbes: an integrated view. *Immunol. Rev.* **219**, 88–102 (2007).
3. Lambeth, J.D. NOX enzymes and the biology of reactive oxygen. *Nat. Rev. Immunol.* **4**, 181–189 (2004).
4. Babior, B.M. NADPH oxidase. *Curr. Opin. Immunol.* **16**, 42–47 (2004).
5. Sumimoto, H. Structure, regulation and evolution of Nox-family NADPH oxidases that produce reactive oxygen species. *FEBS J.* **275**, 3249–3277 (2008).
6. Fang, F.C. Antimicrobial reactive oxygen and nitrogen species: concepts and controversies. *Nat. Rev. Microbiol.* **2**, 820–832 (2004).
7. Singh, A., Zarember, K.A., Kuhns, D.B. & Gallin, J.I. Impaired priming and activation of the neutrophil NADPH oxidase in patients with IRAK4 or NEMO deficiency. *J. Immunol.* **182**, 6410–6417 (2009).
8. Woollard, K.J. & Geissmann, F. Monocytes in atherosclerosis: subsets and functions. *Nat. Rev. Cardiol.* **7**, 77–86 (2009).
9. Finkel, T. Radical medicine: treating ageing to cure disease. *Nat. Rev. Mol. Cell Biol.* **6**, 971–976 (2005).
10. Conley, M.E. *et al.* Genetic analysis of patients with defects in early B-cell development. *Immunol. Rev.* **203**, 216–234 (2005).
11. Winkelstein, J.A. *et al.* X-linked agammaglobulinemia: report on a United States registry of 201 patients. *Medicine (Baltimore)* **85**, 193–202 (2006).
12. Mohamed, A.J. *et al.* Bruton's tyrosine kinase (Btk): function, regulation, and transformation with special emphasis on the PH domain. *Immunol. Rev.* **228**, 58–73 (2009).
13. Gray, P. *et al.* MyD88 adapter-like (Mal) is phosphorylated by Bruton's tyrosine kinase during TLR2 and TLR4 signal transduction. *J. Biol. Chem.* **281**, 10489–10495 (2006).
14. Doyle, S.L., Jefferies, C.A., Feighery, C. & O'Neill, L.A. Signaling by Toll-like receptors 8 and 9 requires Bruton's tyrosine kinase. *J. Biol. Chem.* **282**, 36953–36960 (2007).
15. Mangla, A. *et al.* Pleiotropic consequences of Bruton tyrosine kinase deficiency in myeloid lineages lead to poor inflammatory responses. *Blood* **104**, 1191–1197 (2004).
16. Fiedler, K. *et al.* Neutrophil development and function critically depend on Bruton tyrosine kinase in a mouse model of X-linked agammaglobulinemia. *Blood* **117**, 1329–1339 (2011).
17. Conley, M.E. *et al.* Primary B cell immunodeficiencies: comparisons and contrasts. *Annu. Rev. Immunol.* **27**, 199–227 (2009).
18. Kerner, J.D. *et al.* Impaired expansion of mouse B cell progenitors lacking Btk. *Immunity* **3**, 301–312 (1995).
19. Khan, W.N. *et al.* Defective B cell development and function in Btk-deficient mice. *Immunity* **3**, 283–299 (1995).
20. O'Neill, L.A.J. & Bowie, A.G. The family of five: TIR-domain-containing adaptors in Toll-like receptor signalling. *Nat. Rev. Immunol.* **7**, 353–364 (2007).
21. Piao, W. *et al.* Tyrosine phosphorylation of MyD88 adapter-like (Mal) is critical for signal transduction and blocked in endotoxin tolerance. *J. Biol. Chem.* **283**, 3109–3119 (2008).
22. Jenkins, K.A. & Mansell, A. TIR-containing adaptors in Toll-like receptor signalling. *Cytokine* **49**, 237–244 (2010).
23. Taneichi, H. *et al.* Toll-like receptor signaling is impaired in dendritic cells from patients with X-linked agammaglobulinemia. *Clin. Immunol.* **126**, 148–154 (2008).
24. Pérez de Diego, R. *et al.* Bruton's tyrosine kinase is not essential for LPS-induced activation of human monocytes. *J. Allergy Clin. Immunol.* **117**, 1462–1469 (2006).
25. Horwood, N.J. *et al.* Bruton's tyrosine kinase is required for TLR2 and TLR4-induced TNF, but not IL-6, production. *J. Immunol.* **176**, 3635–3641 (2006).
26. Marron, T.U., Rohr, K., Martinez-Gallo, M., Yu, J. & Cunningham-Rundles, C. TLR signaling and effector functions are intact in XLA neutrophils. *Clin. Immunol.* **137**, 74–80 (2010).
27. Honda, F. *et al.* Transducible form of p47phox and p67phox compensate for defective NADPH oxidase activity in neutrophils of patients with chronic granulomatous disease. *Biochem. Biophys. Res. Commun.* **417**, 162–168 (2012).
28. Dang, P.M. *et al.* A specific p47phox -serine phosphorylated by convergent MAPKs mediates neutrophil NADPH oxidase priming at inflammatory sites. *J. Clin. Invest.* **116**, 2033–2043 (2006).
29. Scapini, P., Pereira, S., Zhang, H. & Lowell, C.A. Multiple roles of Lyn kinase in myeloid cell signaling and function. *Immunol. Rev.* **228**, 23–40 (2009).
30. Zhu, Q.S. *et al.* G-CSF induced reactive oxygen species involves Lyn-PI3-kinase-Akt and contributes to myeloid cell growth. *Blood* **107**, 1847–1856 (2006).
31. Pereira, S. & Lowell, C. The Lyn tyrosine kinase negatively regulates neutrophil integrin signaling. *J. Immunol.* **171**, 1319–1327 (2003).
32. Vlahos, C.J., Matter, W.F., Hui, K.Y. & Brown, R.F. A specific inhibitor of phosphatidylinositol 3-kinase, 2-(4-morpholinyl)-8-phenyl-4H-1-benzopyran-4-one (LY294002). *J. Biol. Chem.* **269**, 5241–5248 (1994).
33. Sadhu, C., Masinovsky, B., Dick, K., Sowell, C.G. & Staunton, D.E. Essential role of phosphoinositide 3-kinase δ in neutrophil directional movement. *J. Immunol.* **170**, 2647–2654 (2003).
34. Morris, A.C. *et al.* C5a-mediated neutrophil dysfunction is RhoA-dependent and predicts infection in critically ill patients. *Blood* **117**, 5178–5188 (2011).
35. Santos-Sierra, S. *et al.* Mal connects TLR2 to PI3Kinase activation and phagocyte polarization. *EMBO J.* **28**, 2018–2027 (2009).
36. Nam, S. *et al.* Action of the Src family kinase inhibitor, dasatinib (BMS-354825), on human prostate cancer cells. *Cancer Res.* **65**, 9185–9189 (2005).
37. Lai, J.Y. *et al.* Potent small molecule inhibitors of spleen tyrosine kinase (Syk). *Bioorg. Med. Chem. Lett.* **13**, 3111–3114 (2003).
38. Slack-Davis, J.K. *et al.* Cellular characterization of a novel focal adhesion kinase inhibitor. *J. Biol. Chem.* **282**, 14845–14852 (2007).
39. Korade-Mirnics, Z. & Corey, S.J. Src kinase-mediated signaling in leukocytes. *J. Leukoc. Biol.* **68**, 603–613 (2000).
40. Bradshaw, J.M. The Src, Syk, and Tec family kinases: distinct types of molecular switches. *Cell. Signal.* **22**, 1175–1184 (2010).
41. Vassilev, A., Ozer, Z., Navara, C., Mahajan, S. & Uckun, F.M. Bruton's tyrosine kinase as an inhibitor of the Fas/CD95 death-inducing signaling complex. *J. Biol. Chem.* **274**, 1646–1656 (1999).
42. Wang, A.V., Scholl, P.R. & Geha, R.S. Physical and functional association of the high affinity immunoglobulin G receptor (FcγRI) with the kinases Hck and Lyn. *J. Exp. Med.* **180**, 1165–1170 (1994).
43. Boyle, K.B. *et al.* Class IA phosphoinositide 3-kinase β and δ regulate neutrophil oxidase activation in response to *Aspergillus fumigatus* hyphae. *J. Immunol.* **186**, 2978–2989 (2011).
44. Kawabuchi, M. *et al.* Transmembrane phosphoprotein Cbp regulates the activities of Src-family tyrosine kinases. *Nature* **404**, 999–1003 (2000).
45. Saito, K. *et al.* BTK regulates PtdIns-4,5-P2 synthesis: importance for calcium signaling and PI3K activity. *Immunity* **19**, 669–678 (2003).
46. Condliffe, A.M. *et al.* Sequential activation of class IB and class IA PI3K is important for the primed respiratory burst of human but not murine neutrophils. *Blood* **106**, 1432–1440 (2005).
47. Uckun, F.M. *et al.* Anti-breast cancer activity of LFM-A13, a potent inhibitor of Polo-like kinase (PLK). *Bioorg. Med. Chem.* **15**, 800–814 (2007).
48. Mahajan, S. *et al.* Rational design and synthesis of a novel anti-leukemic agent targeting Bruton's tyrosine kinase (BTK), LFM-A13 [alpha-cyano-β-hydroxy-β-methyl-N-(2,5-dibromophenyl)propenamide]. *J. Biol. Chem.* **274**, 9587–9599 (1999).

ONLINE METHODS

Reagents and antibodies. The following reagents were used: lipopolysaccharide derived from *Escherichia coli* or *Pseudomonas aeruginosa*, fMLP, PMA, DHR123, luminol, N-acetyl cysteine, aprotinin, leupeptin, pepstatin and phenylmethyl sulfonyl fluoride (all from Sigma-Aldrich); recombinant human TNF (R&D Systems); Pam_3CSK_4, LFM-A13, LFM-A11, Syk inhibitor, FAK inhibitor and Ly294002 (all from Calbiochem); and dasatinib, IC87114 and AS-605240 (all from Biovision). Oligodeoxynucleotide CpG-A (5′-GGT GCATCGATGCAGGGGGG-3′) was from Operon Biotechnologies.

The antibodies used were as follows: goat polyclonal antibody to PI(3)K-p85α phosphorylated at Tyr508 (sc-12929), Hck phosphorylated at Tyr411 (sc-12928), rabbit polyclonal antibody to Hck (N-30), anti-PTEN (FL-403), anti-PTP-PEST (H130), anti-FAK (A-17), anti-Vav (C-14), anti-Syk (C-20), anti-SHP2 (C-18) and anti-SHP 1 (C-19), as well as mouse monoclonal antibody (mAb) to $p47^{phox}$ (D-10), $p40^{phox}$ (D-8) or $p22^{phox}$ (CS-9; all from Santa Cruz). Rabbit polyclonal antibody to p101-PI(3)K (07-281) and to $gp91^{phox}$ (07-024) and anti-Rac2 (07-604), biotin-labeled mouse mAb to phosphorylated tyrosine (4G10), as well as horseradish peroxidase–conjugated antibody to goat IgG (AP-180P) were from Upstate; fluorescein isothiocyanate–conjugated mouse mAb to gp91 (7D5) or goat antibody to mouse IgG (238) were from MBL; and mouse mAb to flotillin-1(18), $p67^{phox}$ (29) or PI(3)K-p85 (U15), and fluorescein isothiocyanate–conjugate mouse isotype-matched IgG antibody (MOPC-21) was from BD Pharmingen. Rabbit polyclonal antibody to PI(3)K-p85 (4292), to Lyn (2732), to Lyn phosphorylated at Tyr507 (2731), to Syk phosphorylated Tyr525-Tyr526 (2711), to Src phosphorylated Tyr416 (2101), to FAK phosphorylated Tyr576-Tyr577 (3281), to $p40^{phox}$ phosphorylated at Thr154 (4311) and to caspase-3 (9662), as well as mouse mAb to proliferating cell nuclear antigen (PC-19), were from Cell Signaling. Rabbit mAb to SOD1 (ep1727y), Mal (ep1231y) and catalase (ep1929), as well as rabbit polyclonal antibody to SOD2 (NB100-1992) and to Yes (NBP1-85369), were from Novus Biologicals. Rabbit polyclonal antibody to Bmx (ab73887), to Bmx phosphorylated at Tyr566 (ab59409), to Lyn phosphorylated at Tyr396 (EP503Y), to Vav phosphorylated at Tyr160 (ab4763) and to Prx1 (ab15571), and mouse mAb to Prx2 (12B1), as well as rabbit mAb to Btk (Y440), to CSK (CSK-04), to SHIP (EP378Y) and to Tec (Y398), were from Abcam. Rat mAb to Mal (TIRAP; sebi-1) was from ENZO Life Sciences. Goat polyclonal antibody to CBP (LS-C14699) was from LIFESPAN; anti-β-actin (Ab1) was from Calbiochem; and horseradish peroxidase–conjugated antibody to mouse IgG (NA931), to rabbit IgG (NA934) or to rat IgG (NA9350) was from GE Healthcare. Alexa Flour 546–anti–rabbit IgG (A11035), Alexa Flour 680–anti–rabbit IgG (A10043), Alexa Flour 594–anti–rat IgG (A21209) and Alexa Flour 488–anti–mouse IgG (A21202) were from Invitrogen. Mouse IgG (015-000-003) and rabbit IgG (011-00000-3) were from Jackson ImmunoResearch. Rat IgG2a (eBR2a) was from eBioscience. Horseradish peroxidase–conjugated streptavidin was from Cell Signaling.

The 482H mAb to Btk has been described[49]. Polyclonal antibody to human Btk was raised in rabbits with a Btk peptide of amino acids 169–187 (ENRNGSLKPGSSHRKTKKPC) conjugated to ovalubumin. The antibody collected was further affinity-purified with that same Btk peptide conjugated to thiol–Sepharose 4B (Pharmacia) and was used for immunoprecipitation in some experiments. The specificity of the antibody was confirmed by immunoblot analysis of lysates of Btk-deficient mononuclear cells. Antibody to phosphorylated Ser345 was generated in rabbits by injection of ovalbumin conjugated to a peptide of $p47^{phox}$ phosphorylated at Ser345 (QARPGPQSpPGSPLEEE, where 'Sp' indicates phosphorylated Ser345 (p-Ser345-pep)). The antibody raised was positively affinity-purified with activated thiol–Sepharose 4B adsorbed with p-Ser345-pep. The antibody was further purified by elimination of the fraction that bound to the same peptide of $p47^{phox}$ without phosphorylation at Ser345 (QARPGPQSPGSPLEEE (Ser345-pep)) by passage through thiol–Sepharose 4B conjugated to Ser345-pep; then, the antibody was used for immunoblot analysis. The specificity of the antibody was confirmed by direct enzyme-linked immunosorbent assay with plates coated with Ser345-pep or p-Ser345-pep and by immunoblot analysis experiments showing blockade of the p-$p47^{phox}$ signal by p-Ser345pep but not by Ser345-pep.

Subjects. Patients with XLA (n = 17) with stable health were studied (ages and Btk mutations, **Supplementary Fig. 3**). Healthy volunteers (n = 18) and patients with CVID (n = 5) were enrolled as healthy controls and disease control, respectively. Written informed consent was obtained from all subjects (or their parents). The study protocol was approved by the ethics committee of the Faculty of Medicine, Tokyo Medical and Dental University.

Isolation of neutrophils, monocytes and lymphocytes. Neutrophils were purified from heparinized peripheral blood by a standard technique. All samples were processed within 12 h of blood collection. Peripheral blood diluted in PBS was layered onto a MonoPoly mixture (Flow Laboratories) and centrifuged at 400*g* for 20 min. Layers with enrichment for neutrophils were collected and further purified to a purity of >97% by immunomagnetic negative selection (StemCell Technologies). Sterile and endotoxin-free conditions were used for all procedures. Monocytes were purified from the mononuclear cell–rich fraction with a human monocyte enrichment kit (StemCell Technologies), and lymphocytes were prepared as described[50].

Measurement of production of ROS. Purified neutrophils were loaded for 5 min at 37 °C with DHR123 (5 μg/ml). Cells were washed and then stimulated for 30 min at 37 °C with PMA (100 ng/ml), and the production of ROS was quantified via flow cytometry by measurement of intracellular rhodamine (FACSCalibur; Becton Dickinson). DHR123-loaded neutrophils were also stimulated for 60 min at 37 °C with a TLR ligand (lipopolysaccharide from *E. coli* or *P. aeruginosa*; 100 ng/ml), CpG-A (100 ng/ml) or TNF (1 μg/ml). After incubation, treated and untreated neutrophils were incubated for 5 min at 37 °C with or without fMLP (1 μM), followed by flow cytometry. Results are presented as MFI of treated cells – MFI of untreated cells.

Production of ROS was quantified by standard chemiluminescence. Neutrophils (1.0×10^6) were suspended in 0.5 ml PBS containing luminol (10 μM) preheated to 37 °C. After a baseline measurement was obtained, cells were stimulated with a TLR agonist and then with fMLP (1 μM) or with PMA (100 ng/ml); luminescence signals were monitored throughout the reaction.

Detection of apoptosis. Apoptotic cells were identified by staining with annexin V–fluorescein isothiocyanate and 7-AAD (7-amino-actinomycin D; BD Biosciences). Apoptosis was also identified by immunoblot analysis through the detection of cleaved caspase-3 or degraded proliferating cell nuclear antigen.

Flow cytometry. A FACSCalibur (Beckton Dickenson) was used for all flow cytometry analyzing surface expression of gp91, DHR123 staining, annexin V–7-AAD staining, and JC-1 mitochondrial membrane detection as described[50]. All analyses were undertaken after calibration of the fluorescence intensity with CaliBRITE Beads (BD Biosciences).

Subcellular fractionation of neutrophils. Isolated neutrophils were resuspended at a density of 5×10^7 cells per ml in ice-cold sonication buffer (HEPES (10 mM), pH 7.2, sucrose (0.15 M), EGTA (1 mM), EDTA (1 mM), NaF (25 mM), leupeptin (10 μg/ml), pepstatin (10 μg/ml), aprotinin (1 μg/ml) and PMSF (1 mM)). After sonication and pelleting on ice, 200 μl supernatant was layered on a discontinuous sucrose gradient consisting of 200 μl of 52% (wt/vol) sucrose, 200 μl of 40% (wt/vol) sucrose and 200 μl of 15% (wt/vol) sucrose. After centrifugation (100,000*g* for 60 min), 160 μl supernatant (cytosol source) and 120 μl interface of the 15%–40% sucrose layers (plasma-membrane source) were collected.

Immunoprecipitation and immunoblot analysis. Lysates were prepared from monocytes and lymphocytes as described[51]. For the preparation of lysates from neutrophils, cells were resuspended in lysis buffer (Tris-HCl (50 mM), pH 7.5, NaCl (150 mM), sucrose (0.25 M), EGTA (5 mM), EDTA (5 mM), leupeptin (15 μg/ml), pepstatin (10 μg/ml), aprotinin (10 μg/ml), PMSF (2.5 mM), 1.0% Nonidet-P40, 0.25% sodium deoxycholate, sodium pyrophosphate (10 mM), NaF (25 mM), Na_3VO_4 (5 mM), β-glycerophosphate (25 mM) and DNase I (1 μg/ml)), incubated for 30 min on ice and centrifuged at 15,000*g* for 30 min at 4 °C, then supernatants were collected. For extraction of the membrane-raft fraction, 1% n-dodecyl-β-D-maltoside was added to the lysis buffer. Immunoprecipitation and immunoblot analysis were done as described[52]. For immunoprecipitation of cytosolic proteins from neutrophils, cytosolic proteins obtained as described above were diluted in four volumes of immunoprecipitation buffer (Tris-HCl (20 mM), pH 7.5, NaCl (150 mM), sucrose (0.25 M), EGTA (5 mM), EDTA (5 mM), leupeptin (15 μg/ml), pepstatin (10 μg/ml), aprotinin (10 μg/ml), PMSF (2.5 mM), 0.5% Triton-X, sodium pyrophosphate (10 mM), NaF (25 mM), Na_3VO_4 (5 mM), β-glycerophosphate (50 mM) and levamisole (1 mM)); supernatants were used for immunoprecipitation.

Measurement of phosphatidylinositol-(3,4,5)-trisphosphate. Phosphatidylinositol-(3,4,5)-trisphosphate in unstimulated neutrophils prepared from healthy controls and patients with XLA was measured with an enzyme-linked immunosorbent assay kit in accordance with the manufacturer's instructions (K-2500; Echelon).

Immunofluorescence staining. Cytospin preparations of neutrophils were air-dried and fixed for 10 min with paraformaldehyde in PBS, pH 7.4, then were made permeable for 20 min at −20 °C with acetone, washed, and incubated with the appropriate antibodies. After labeling and washing with 0.2% BSA in PBS, coverslips were mounted with Fluoromount G and the prepared specimens. Nuclei were counterstained with DAPI (4,6-diamidino-2-phenylindole). Slides were analyzed with a fluorescence microscope (FV10i; Olympus) equipped with Fluoview viewer and review station (Olympus). At least 100 cells were inspected for each slide.

Generation of Hph-1-Btk, Hph-1-Btk mutants, and transduction of recombinant protein into cells. Hph-1–tagged Btk constructs were generated by amplification of a full-length Btk cDNA fragment with the appropriate primers (**Supplementary Table 1a**). After the sequence of each PCR product was verified by DNA sequencing, the fragment was ligated into sites of a pET28b vector (Merck) cleaved by *Xma1* and *Sal1*; the vector has a six-histidine site for protein purification and two tandem Hph-1 sequences for protein transduction. Constructs with deletion of the Tec homology domain, SH3 domain or SH2 domain were generated by mutagenesis with the QuikChange SiteDirected Mutagenesis Kit (Stratagene) and the appropriate primers (**Supplementary Table 1b**). The Hph-1-Gal4 construct has been described[52]. Proteins were induced in BL21 Star competent cells (Novagen) as described[52]. Proteins were treated with Detoxi-Gel Endotoxin Removing Gel (Takara Bio) for elimination of endotoxins and were frozen at −80 °C until further use. Neutrophils (1×10^6 per ml) were incubated for 1 h with 1 μM Hph-1–tagged proteins (80 μg recombinant Hph-1–tagged full-length-Btk was used for 1×10^6 neutrophils for transduction at a concentration of 1 μM) and washed, then ROS production was assayed.

Btk-precipitation assay. Lysates of neutrophils from healthy controls were prepared on ice for 30 min with immunoprecipitation lysis buffer. Supernatants were then treated with protein G beads (GE Health Care) for removal of immunoglobulin G from the neutrophil lysate. For the Btk-precipitation assay, purified Btk recombinant proteins or control recombinant protein were eluted and proteins were measured by BCA protein assay (Pierce). Bacterial supernatants were bound to nickel–nitrilotriacetic acid Sepharose beads (Qiagen) and bound recombinant proteins were eluted, then equimolar amounts of recombinant proteins were rebound to the nickel beads; afterward, samples were washed and then incubated overnight at 4 °C with the cell lysates. Beads were washed four times with lysis buffer and assessed by immunoblot analysis with anti-Mal. Before incubation with cell lysates, the amount of the recombinant protein rebound to nickel beads was assessed by immunoblot analysis with anti-histidine, and the 'dose' was readjusted for further precipitation assays.

Statistical analysis. Student's t-test was used for statistical analysis. The software GraphPad Prism 4 was used for these analyses.

49. Futatani, T. *et al.* Deficient expression of Bruton's tyrosine kinase in monocytes from X-linked agammaglobulinemia as evaluated by a flow cytometric analysis and its clinical application to carrier detection. *Blood* **91**, 595–602 (1998).
50. Takahashi, N. *et al.* Impaired CD4 and CD8 effector function and decreased memory T cell populations in ICOS-deficient patients. *J. Immunol.* **182**, 5515–5527 (2009).
51. Morio, T. *et al.* Ku in the cytoplasm associates with CD40 in human B cells and translocates into the nucleus following incubation with IL-4 and anti-CD40 mAb. *Immunity* **11**, 339–348 (1999).
52. Choi, J.M. *et al.* Intranasal delivery of the cytoplasmic domain of CTLA-4 using a novel protein transduction domain prevents allergic inflammation. *Nat. Med.* **12**, 574–579 (2006).

An Inv(16)(p13.3q24.3)-Encoded *CBFA2T3-GLIS2* Fusion Protein Defines an Aggressive Subtype of Pediatric Acute Megakaryoblastic Leukemia

Tanja A. Gruber,[1,6,8] Amanda Larson Gedman,[6] Jinghui Zhang,[2,8] Cary S. Koss,[1] Suresh Marada,[3] Huy Q. Ta,[6] Shann-Ching Chen,[7] Xiaoping Su,[2,25] Stacey K. Ogden,[3] Jinjun Dang,[6] Gang Wu,[2] Vedant Gupta,[1] Anna K. Andersson,[6] Stanley Pounds,[5] Lei Shi,[5] John Easton,[8] Michael I. Barbato,[8] Heather L. Mulder,[8] Jayanthi Manne,[8] Jianmin Wang,[4,8] Michael Rusch,[2,8] Swati Ranade,[24] Ramapriya Ganti,[6] Matthew Parker,[2] Jing Ma,[7] Ina Radtke,[6] Li Ding,[8,11] Giovanni Cazzaniga,[13] Andrea Biondi,[14] Steven M. Kornblau,[9] Farhad Ravandi,[10] Hagop Kantarjian,[10] Stephen D. Nimer,[15] Konstanze Döhner,[16] Hartmut Döhner,[16] Timothy J. Ley,[8,11,12] Paola Ballerini,[17] Sheila Shurtleff,[6] Daisuke Tomizawa,[20] Souichi Adachi,[21] Yasuhide Hayashi,[22] Akio Tawa,[23] Lee-Yung Shih,[18] Der-Cherng Liang,[19] Jeffrey E. Rubnitz,[1] Ching-Hon Pui,[1] Elaine R. Mardis,[8,11,12] Richard K. Wilson,[8,11,12] and James R. Downing[6,8,*]

[1]Department of Oncology
[2]Department of Computational Biology
[3]Department of Biochemistry
[4]Information Sciences
[5]Department of Biostatistics
[6]Department of Pathology
[7]Hartwell Center for Biotechnology and Bioinformatics
[8]St. Jude Children's Research Hospital, Washington University Pediatric Cancer Genome Project
St. Jude Children's Research Hospital, Memphis, TN 38105, USA
[9]Department of Blood and Marrow Transplantation
[10]Department of Leukemia
University of Texas MD Anderson Cancer Center, Houston, TX 77030, USA
[11]The Genome Institute at Washington University
[12]Siteman Cancer Center
Washington University School of Medicine, St. Louis, MO 63110, USA
[13]Centro Ricerca Tettamanti, Pediatric Clinic, University of Milan-Bicocca, 20052 Monza, Italy
[14]Pediatric Unit, University of Milan-Bicocca, San Gerardo Hospital, 20900 Monza, Italy
[15]Molecular Pharmacology and Chemistry Program, Sloan Kettering Institute, New York, NY 10065, USA
[16]Department of Internal Medicine III, University of Ulm, 89081 Ulm, Germany
[17]Laboratoire d'Hématologie, Hôpital A. Trousseau, 75012 Paris, France
[18]Division of Hematology-Oncology, Department of Internal Medicine, Chang Gung Memorial Hospital, Chang Gung University, Taipei 105, Taiwan
[19]Division of Pediatric Hematology Oncology, Mackay Memorial Hospital, Taipei 104, Taiwan
[20]Department of Pediatrics, Tokyo Medical and Dental University, Tokyo 113-8510, Japan
[21]Human Health Sciences, Graduate School of Medicine, Kyoto University, Kyoto 606-8501, Japan
[22]Department of Haematology/Oncology, Gunma Children's Medical Center, Shibukawa 377-8577, Japan
[23]Department of Pediatrics, National Hospital Organization Osaka National Hospital, Osaka 540-0006, Japan
[24]Pacific Biosciences, Menlo Park, CA 94025, USA
[25]Present address: Department of Bioinformatics and Computational Biology, University of Texas MD Anderson Cancer Center, Houston, TX 77030, USA
*Correspondence: james.downing@stjude.org
http://dx.doi.org/10.1016/j.ccr.2012.10.007

SUMMARY

To define the mutation spectrum in non-Down syndrome acute megakaryoblastic leukemia (non-DS-AMKL), we performed transcriptome sequencing on diagnostic blasts from 14 pediatric patients and validated our findings in a recurrency/validation cohort consisting of 34 pediatric and 28 adult AMKL samples. Our analysis identified a cryptic chromosome 16 inversion (inv(16)(p13.3q24.3)) in 27% of pediatric cases, which encodes a CBFA2T3-GLIS2 fusion protein. Expression of CBFA2T3-GLIS2 in *Drosophila* and murine hematopoietic cells induced bone morphogenic protein (BMP) signaling and resulted in a marked increase in the self-renewal capacity of hematopoietic progenitors. These data suggest that expression of CBFA2T3-GLIS2 directly contributes to leukemogenesis.

Significance

Acute megakaryoblastic leukemia (AMKL) accounts for 10% of childhood acute myeloid leukemia (AML). Although AMKL patients with Down syndrome (DS-AMKL) have an excellent survival, non-DS-AMKL patients have an extremely poor outcome with a 3 year survival of less than 40%. With the exception of the t(1;22) seen in the majority of infants with non-DS-AMKL, little is known about the molecular lesions that underlie this leukemia subtype. Our results identified a fusion gene, *CBFA2T3-GLIS2*, that functions as a driver mutation in a subset of these patients. Importantly, pediatric patients with *CBFA2T3-GLIS2* expressing AMKL had inferior outcomes (5 year survival 34.3% versus 88.9%; p = 0.03), demonstrating that this lesion is a prognostic factor in this leukemia population.

INTRODUCTION

Acute megakaryoblastic leukemia (AMKL) accounts for approximately 10% of pediatric acute myeloid leukemia (AML) and 1% of adult AML (Athale et al., 2001; Barnard et al., 2007; Oki et al., 2006; Tallman et al., 2000). AMKL is divided into two subgroups: AMKL arising in patients with Down syndrome (DS-AMKL), and leukemia arising in patients without Down syndrome (non-DS-AMKL). Although DS-AMKL patients have an excellent prognosis with an ~80% survival, non-DS-AMKL patients do not fare as well, with a reported survival of only 14%–34% despite high-intensity chemotherapy (Athale et al., 2001; Barnard et al., 2007; Creutzig et al., 2005). With the exception of the t(1;22) seen in infant non-DS-AMKL, little is known about the molecular lesions that underlie this leukemia subtype (Carroll et al., 1991; Lion et al., 1992; Ma et al., 2001; Mercher et al., 2001).

We recently reported data from a high-resolution study of DNA copy number abnormalities (CNAs) and loss of heterozygosity on pediatric de novo AML (Radtke et al., 2009). These analyses demonstrated a very low burden of genomic alterations in all pediatric AML subtypes except AMKL. AMKL cases were characterized by complex chromosomal rearrangements and a high number of CNAs. To define the functional consequences of the identified chromosomal rearrangements in non-DS-AMKL, the St. Jude Children's Research Hospital-Washington University Pediatric Cancer Genome Project performed transcriptome and exome sequencing on diagnostic leukemia samples.

RESULTS

AMKL Is Characterized by Chimeric Transcripts

Transcriptome sequencing was performed on diagnostic leukemia cells from 14 pediatric non-DS-AMKL patients (discovery cohort) (see Tables S1 and S2 available online). Our analysis identified structural variations (SVs) that resulted in the expression of chimeric transcripts encoding fusion proteins in 12 of 14 cases (Table S3). Remarkably, in 7 of 14 cases, a cryptic inversion on chromosome 16 (inv(16)(p13.3q24.3)) was detected that resulted in the joining of *CBFA2T3*, a member of the ETO family of nuclear corepressors, to *GLIS2*, a member of the GLI family of transcription factors (Figures 1, 2, and S1). In six of these cases, exon 10 of *CBFA2T3* was fused to exon 3 of *GLIS2*, whereas in the remaining one case, exon 11 of *CBFA2T3* was fused to exon 1 of *GLIS2*. Both encoded proteins retain the three CBFA2T3 N-terminal *nervy* homology regions that mediate protein interactions and the five GLIS2 C-terminal zinc finger domains that bind the *Glis* DNA consensus sequence (Figures 1A and 1B). Whole-genome sequence analysis of tumor and germline DNA from four cases demonstrated that the *CBFA2T3-GLIS2* chimeric gene resulted from simple balanced inversions in three cases and a complex rearrangement involving chromosomes 16 and 9 in the fourth case (Figures 2 and S1).

Chimeric transcripts were also detected in five of seven leukemia samples that lacked expression of *CBFA2T3-GLIS2*, including one case each expressing in-frame fusions of *GATA2-HOXA9*, *MN1-FLI1*, *NIPBL-HOXB9*, *NUP98-KDM5A*, *GRB10-SDK1*, and *C8orf76-HOXA11AS* (Figure 3; Table S3). Importantly, several of the genes involved in these translocations play a direct role in normal megakaryocytic differentiation (*GATA2* and *FLI1*), have been previously shown to be involved in leukemogenesis (*HOXA9*, *MN1*, *HOXB9*, *NUP98*, *KDM5A*), or are highly expressed in hematopoietic stem cells or myeloid/megakaryocytic progenitors (Figure S2) (Argiropoulos and Humphries, 2007; Buijs et al., 2000; Heuser et al., 2011; Kawada et al., 2001; Visvader et al., 1995; Wang et al., 2009). Analysis of a recurrency/validation cohort consisting of diagnostic leukemia cells from 62 AMKL cases (34 pediatric and 28 adult) revealed 6 additional pediatric samples carrying *CBFA2T3-GLIS2* for an overall frequency of 27% (13 of 48) in pediatric AMKL (Table S1). None of the adult AMKL cases contained this chimeric transcript, suggesting that this lesion is restricted to pediatric non-DS-AMKLs. *NUP98-KDM5A* was the only other chimeric transcript that was recurrent, being detected in 8.3% (4 of 48) of pediatric cases (Table S1). This chimeric transcript was also not detected in adult AMKLs.

Cooperating Lesions in AMKL

In addition to the described chimeric transcripts, exome sequence analysis on 10 of the 14 samples in the discovery cohort that had matched germline DNA, coupled with CNAs detected by Affymetrix SNP6 microarrays, revealed an average of 5 (range 1–14) somatic nonsilent sequence mutations and 5 (range 0–11) CNAs involving annotated genes per case. (Tables S4, S5, and S6; Figure S1). Despite the relative paucity of somatic mutations, recurrent lesions were identified in *JAK* kinase genes, *MPL* and *GATA1*, which have been previously shown to play a role in AMKL (Malinge et al., 2008). Sequence analysis of these genes in cases within the recurrency cohort that had available genomic DNA revealed activating mutations in *JAK* kinases (9 of 51, 17.6%) and *MPL* (2 of 51, 3.9%), as well as inactivating mutations in *GATA1* (5 of 51, 9.8%) (Tables S1 and S6). In addition, 7 of 14 cases with available copy number data contained amplification of chromosome 21 in the Down syndrome critical region (DSCR; chr21q22) that includes genes known to play a role in AML such as *RUNX1*, *ETS2*, and *ERG* (Table S4; Figure S1). Three of these cases carry the *CBFA2T3-GLIS2* chimeric gene. Importantly, the total burden of somatic mutations was significantly lower in the *CBFA2T3-GLIS2*-expressing cases (7.17 ± 3.60 versus 16.60 ± 5.13; p = 0.009; Table S5).

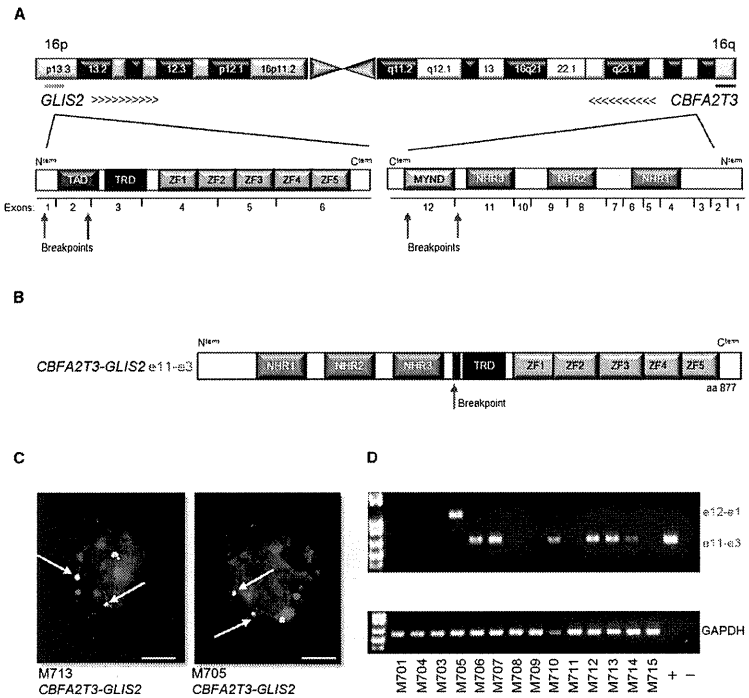

Figure 1. Inv(16)(p13.3;q24.3) Encodes a *CBFA2T3-GLIS2* Chimeric Transcript

(A) Schematic of chromosome 16 with locations of *GLIS2* and *CBFA2T3* shown. Arrows indicate orientation of the gene and the green and red lines the probes used for FISH. The protein structure of the genes is shown below chromosome 16 and is not drawn to scale. Breakpoints are indicated by arrows. TAD, transactivation domain; TRD, transcriptional regulatory domain; ZF, zinc finger; NHR, nervy homology region.

(B) Schematic of CBFA2T3-GLIS2 chimeric protein.

(C) Interphase FISH analysis of two representative patient samples carrying *CBFA2T3-GLIS2*. The *GLIS2* probe is green; the *CBFA2T3* probe is red. White arrows indicate the fusion event. Scale bars, 10 μm.

(D) RT-PCR for CBFA2T3-GLIS2 and GAPDH on the discovery cohort.

See also Figure S1 and Tables S1, S2, S3, S4, S5, and S6.

CBFA2T3-GLIS2 AMKL Is a Distinct Subtype of Pediatric AMKL with a Poor Prognosis

The gene expression profile of *CBFA2T3-GLIS2* AMKL was distinct from that of AMKL cells lacking this chimeric transcript and from other genetic subtypes of pediatric AML (Figures 4A and 4B). A detailed coexpression network analysis of the top 4,000 differentially expressed genes suggests that expression of *CBFA2T3-GLIS2* leads to marked upregulation of *BMP2*, a downstream target of Hedgehog signaling (Figures 4B and S3; Table S7). Moreover, gene set enrichment analysis based on KEGG pathway annotation of the top-scoring network module demonstrated Hedgehog and JAK-STAT pathways to be significantly upregulated in *CBFA2T3-GLIS2*-positive AMKL (Figure S3).

Given the historically poor outcomes seen in pediatric non-DS-AMKL, we next explored whether the presence of *CBFA2T3-GLIS2* identified a clinically distinct subset of cases. Outcome data were available on 40 pediatric patients. Although these patients were treated at a number of different centers using a variety of different therapeutic approaches, the presence of *CBFA2T3-GLIS2* identified a subgroup of patients with a significantly worse overall survival at 5 years as compared to patients with AMKL that lacked this chimeric transcript (28.1% versus 41.9%; p = 0.05; Figure 4C). Moreover, when this analysis was limited to patients treated at a single institution (St. Jude, n = 19), the adverse prognostic impact of *CBFA2T3-GLIS2* on survival was maintained (34.3% versus 88.9%; p = 0.03; Figure 4D).

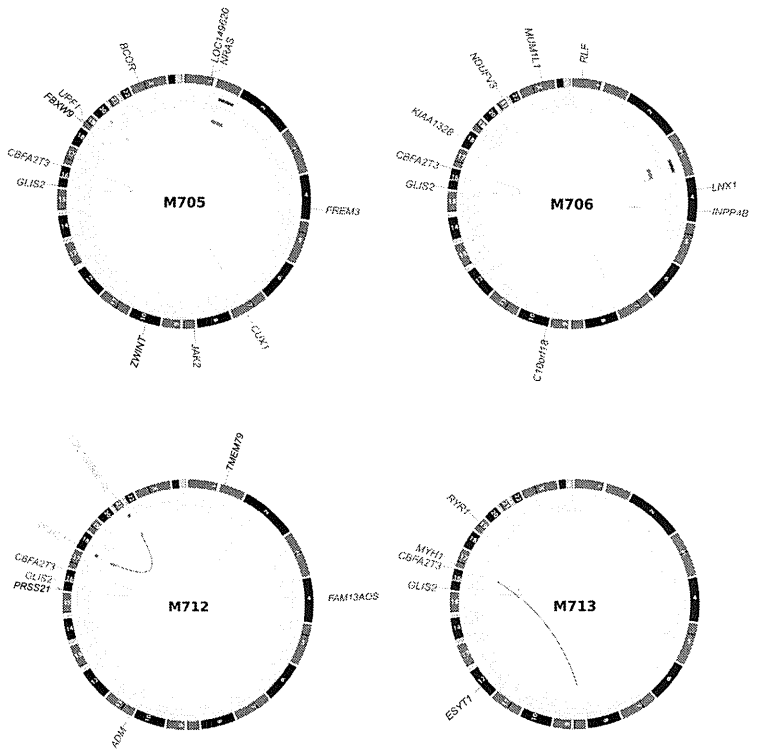

Figure 2. Somatic Mutations in Whole-Genome-Sequenced AMKL Cases

Plots depict structural genetic variants, including DNA copy number alterations, intra- and interchromosomal translocations, and sequence alterations (Krzywinski et al., 2009). DNA copy number alterations: loss of heterozygosity (LOH), orange; amplification, red; deletion, blue. Sequence mutations in Refseq genes: silent SNVs (SNVs), black; UTR, brown; nonsilent SNVs, blue. Genes at structural variant breakpoints: genes involved in in-frame fusions, red; others, green.

CBFA2T3-GLIS2-Modified Hematopoietic Cells Demonstrate Enhanced Self-Renewal

CBFA2T3 (also known as *MTG16*) was initially identified as a fusion partner with *RUNX1* in rare cases of therapy-related AML that contain a t(16;21)(q24;q22) (Gamou et al., 1998). More recently, CBFA2T3 has been implicated in the maintenance of hematopoietic stem cell quiescence (Chyla et al., 2008). By contrast, to our knowledge, GLIS2 has not been previously implicated in leukemogenesis. GLIS2 is a member of the GLI-similar (GLIS1-3) subfamily of Krüppel-like zinc finger transcription factors and is closely related to the GLI family of transcription factors that function as critical elements of the hedgehog signaling pathway (Kim et al., 2007; Lamar et al., 2001). GLIS2 is expressed in the kidney, and germline-inactivating mutations lead to nephronophthisis, an autosomal recessive cystic kidney disease (Attanasio et al., 2007). Although *GLIS2* is not normally expressed in the hematopoietic system, its fusion to *CBFA2T3* as a result of the inv(16)(p13.3q24.3) results in high-level expression of the C-terminal portion of the protein including its DNA-binding domain (Figure S1).

To explore the functional effects of the CBFA2T3-GLIS2 fusion protein, we transduced murine hematopoietic cells with a retrovirus expressing either *CBFA2T3-GLIS2* or *GLIS2* alone and assessed their effect on in vitro colony formation, differentiation, and replating efficiency as a surrogate measure of self-renewal (Figures 5A and 5B). On the initial plating, the expression of CBFA2T3-GLIS2 had no effect on colony numbers, size, or overall myeloid/erythroid differentiation when cells were grown in the presence of IL3, IL6, SCF, and EPO. However, hematopoietic cells transduced with the empty

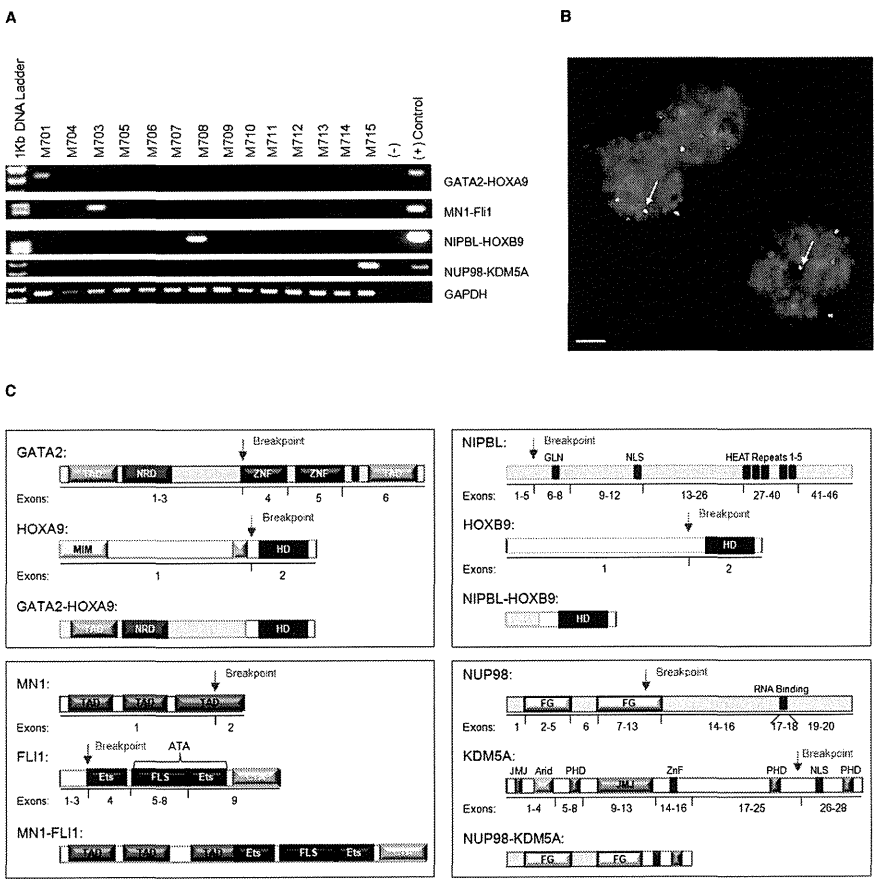

Figure 3. Low-Frequency Chimeric Transcripts in Pediatric AMKL

Four chimeric transcripts were identified in one case each of the discovery cohort and tested for in the recurrency cohort: *GATA2-HOXA9*, *MN1-FLI1*, *NIPBL-HOXB9*, and *NUP98-KDM5A*.

(A) RT-PCR validation of the discovery cohort. Primers and conditions are described in Supplemental Experimental Procedures.

(B) Interphase FISH analysis of M703 carrying the MN1-FLI1 chimeric protein. The *MN1* probe is red; the *FLI1* probe is green. White arrows indicate the fusion event. Scale bar, 10 μm.

(C) Schematic of chimeric proteins. Exons and domains are not drawn to scale. NRD, negative regulatory domain; ZNF, zinc finger; MIM, Meis interaction motif; HD, Hox domain; Ets, E-twenty six domain; FLS, Fli1-specific region; CTA, C-terminal transactivation domain; GLN, glutamine-rich domain; NLS, nuclear-localizing signal; HEAT, *H*untingtin/*E*F3/PP2*A*/*T*OR1 domain; FG, phenylalanine-glycine repeats; JMJ, jumonji domain; ARID, AT-rich interaction domain; PHD, plant homeodomain. See also Figure S2.

retrovirus (MSCV-IRES-mCherry [MIC]) failed to form colonies after the second replating, whereas expression of either CBFA2T3-GLIS2 or wild-type GLIS2 resulted in a marked increase in the self-renewal capacity, with colony formation persisting through ten replatings (Figure 5C). Upon serial replating, two colony types were detected: CFU-GM and CFU-Meg

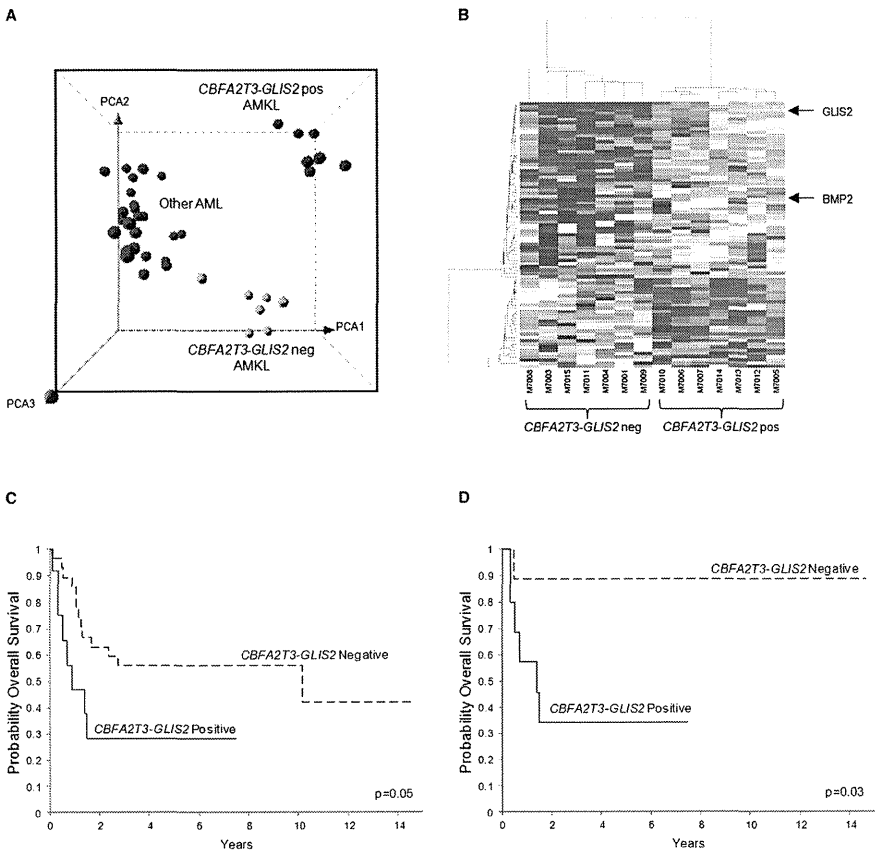

Figure 4. *CBFA2T3-GLIS2* Defines a Unique Subtype of AML with a Distinct Gene Expression Signature and Poor Outcomes

(A) Principal component analysis of the gene expression profiles of the AMKL discovery cohort and 32 other non-AMKL AML samples representing all other known genetic subtypes of pediatric AML. Clusters were generated using 1,000 genes selected by k-means algorithm. A detailed description of the samples included in this analysis can be found at NCBI Gene Expression Omnibus, accession GSE35203.

(B) Heatmap of differentially expressed genes in the top-scoring network module of CBFA2T3-GLIS2-positive (pos) and -negative (neg) AMKL patient samples. For gene relationships, please see Figure S3. For a detailed list of the top 500 differentially expressed genes (not limited to this network), please see Table S7.

(C) Overall survival of 40 pediatric non-DS AMKL cases treated at multiple institutions (*CBFA2T3-GLIS2*-negative cases n = 28, and *CBFA2T3-GLIS2*-expressing cases, n = 12). The curves for the two groups were tested by log rank method and exact test using permutation that yielded a p value of 0.05.

(D) Overall survival of 19 pediatric non-DS AMKL cases treated at St. Jude Children's Research Hospital (*CBFA2T3-GLIS2*-negative cases, n = 9, and *CBFA2T3-GLIS2*-expressing cases, n = 10). The curves for the two groups were tested by log rank method and exact test using permutation that yielded a p value of 0.03. See also Figure S3 and Table S7.

(Figure 5D). Immunophenotypic analysis at the third replating also revealed evidence of megakaryocytic differentiation with CD41/CD61 dual expression and the absence of cKIT and Sca1 expression in the majority of cells (Figure 5E). Importantly, CBFA2T3-GLIS2-expressing cells remained growth factor dependent, suggesting that cooperating mutations in growth factor

signaling pathways are likely required for full leukemic transformation (data not shown). Moreover, transplantation of *CBFA2T3-GLIS2*-transduced bone marrow cells into syngeneic recipients failed to induce overt leukemia at day 365 as demonstrated by normal blood counts and low-level reporter gene expression in peripheral blood (<5%) (data not shown), consistent with a requirement for cooperative mutations. Failure to induce leukemia in mice as a single lesion has been previously reported for other chimeric genes that confer the ability to serially replate in colony-forming assays, including *AML1-ETO* (Higuchi et al., 2002).

CBFA2T3-GLIS2 Induces BMP Signaling

GLIS2 can function as both a transcriptional activator and repressor depending on the cellular context and has been implicated in altered signaling through a number of pathways including sonic hedgehog-GLI1 (SHH) and WNT/β-catenin (Attanasio et al., 2007; Kim et al., 2007). Analysis of the gene expression signatures of *CBFA2T3-GLIS2* expressing AMKLs revealed altered expression of a number of genes in the SHH and WNT pathways, as well as genes in the bone morphogenic protein (BMP) pathway, which is directly influenced by SHH signaling (Figures 4B, 6A, and S3) (Dahn and Fallon, 2000; Ingham and McMahon, 2001; Vokes et al., 2007). When this analysis was limited to genes containing GLI consensus DNA-binding sites (Gli-BS) in their promoters or to genes known to be transcriptional targets of GLIS2, marked overexpression of *PTCH1*, *HHIP*, *BMP2*, and *BMP4* was observed (Figures 6B, S3, and S4; Table S7) (Attanasio et al., 2007). Consistent with this observation, although CBFA2T3-GLIS2 only weakly activated transcription of a reporter construct containing the Gli-BS (Figure S4), it strongly activated transcription of the Gli-BS-containing BMP4 promoter-driven luciferase construct and induced expression of BMP4 in murine hematopoietic cells (Figures 6C and S4). Moreover, CBFA2T3-GLIS2 strongly activated a BMP response element (BRE) containing luciferase reporter construct and induced expression of the BMP downstream transcriptional target, inhibitor of differentiation 1 (*ID1*) (Korchynskyi and ten Dijke, 2002), consistent with the induced expression of BMP2/BMP4 (Figure S4).

BMP signaling plays a critical role in the specification of hematopoiesis in developing embryos, and studies suggest that BMP4 stimulation can augment megakaryocytic output from CD34 progenitors (Jeanpierre et al., 2008; Söderberg et al., 2009). To determine if the observed CBFA2T3-GLIS2-induced BMP expression contributes to the enhanced replating capacity of murine hematopoietic cells, colony-replating assays were repeated in the presence of dorsomorphin, a selective small molecule inhibitor of the BMP type I receptors that blocks BMP-mediated phosphorylation of SMAD 1/5/8 (Yu et al., 2008). Importantly, CBFA2T3-GLIS2 as well as GLIS2-expressing hematopoietic cells were significantly more sensitive to dorsomorphin than wild-type cells in the first plating (Figure 6D). Continuous exposure to dorsomorphin inhibited colony formation in a dose-dependent manner on subsequent platings (data not shown). Interestingly, sublethal doses of dorsomorphin in *CBFA2T3-GLIS2*-positive cells led to an upregulation of *Bmp4* and *Id1* transcripts over time, with colony counts returning to untreated levels, suggesting that cells are able to overcome this inhibition by upregulating the BMP pathway (data not shown).

To further explore the downstream signaling of CBFA2T3-GLIS2 in human leukemia cell lines, we first assessed the expression level of *GLIS2* in human cancer cell lines using the recently published Broad-Novartis Cancer Cell Line Encyclopedia (Figure 7A) (Barretina et al., 2012). Interestingly, this analysis showed that GLIS2 expression levels are lowest in leukemia cell lines. Moreover, within the leukemias, the highest expressing cell line was the pediatric AMKL cell line M07e. To further explore AMKL cell lines, we performed RT-PCR for *CBFA2T3-GLIS2* on five human AMKL cell lines. Three of the five cell lines (RS1, WSU-AML, and M07e) expressed *CBFA2T3-GLIS2* (Figure 7B). The presence of the chimeric gene in these lines was validated by FISH analysis (Figure 7B). We went on to determine the relative expression of BMP genes by semiquantitative RT-PCR and found a trend toward upregulation of these genes in the CBFA2T3-GLIS2-positive cells (Figure 7C). We also assessed our AMKL cell lines for dorsomorphin sensitivity and found a trend toward increased sensitivity in cell lines expressing *CBFA2T3-GLIS2* as determined by a standard MTT assay (Figure 7D).

To determine if CBFA2T3-GLIS2 induces the upregulation of BMP signaling in vivo, we generated transgenic *Drosophila* expressing either *CBFA2T3-GLIS2* or full-length *GLIS2* using an epithelial promoter and examined their effect on fly development. During *Drosophila* development, the WNT, BMP, and SHH homologs (Wg, Dpp, and Hh, respectively) have distinct roles in patterning adult wing structures (Dahn and Fallon, 2000; Ingham and McMahon, 2001; Vokes et al., 2007). When altered, these signaling pathways trigger characteristic loss- and gain-of-function phenotypes (Tabata and Takei, 2004). Expression of CBFA2T3-GLIS2 and full-length GLIS2 in *Drosophila* resulted in ectopic expression of endogenous *dpp*, the fly homolog of *BMP4*, in wing imaginal discs (Figures 8A and S5). Immunofluorescence confirmed the nuclear localization of CBFA2T3-GLIS2 (Figure 8A). Both CBFA2T3-GLIS2 and GLIS2 overexpression induced lethality. However, a small number of escapers developed to pharate adults and demonstrated a morphologic *dpp* gain-of-function phenotype; wing hinges were converted to notum, and legs were shortened and broadened (Figure 8B) (Grieder et al., 2009). Rare *CBFA2T3-GLIS2* transgenic flies developed to adulthood and demonstrated mild ectopic venation throughout the wing blade, as well as wing blistering consistent with a *dpp* gain-of-function phenotype (Figure 8B) (Sander et al., 2010).

DISCUSSION

Sequence analysis of pediatric non-DS-AMKLs revealed the expression of an inv(16)-encoded *CBFA2T3-GLIS2* in almost 30% of pediatric non-DS-AMKL patients, and its presence defined a distinct subgroup of patients that had an exceptionally poor outcome when compared to patients with AMKL that lacked this lesion. In addition, five other chimeric transcripts (*GATA2-HOXA9*, *MN1-FLI1*, *NIPBL-HOXB9*, *GRB10-SDK1*, and *C8orf76-HOXA11AS*) were detected in single AMKL cases. Surprisingly, none of the identified chimeric transcripts was detected in adult AMKL cases, highlighting the significant

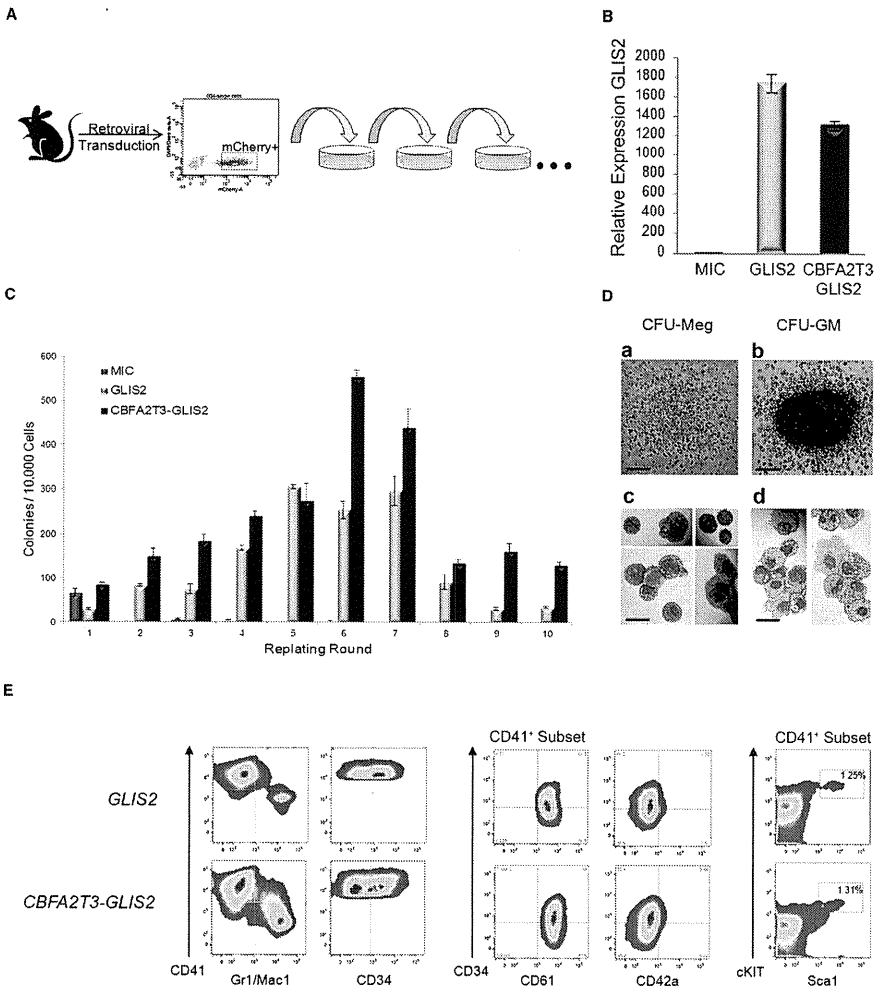

Figure 5. *CBFA2T3-GLIS2* Leads to Enhanced Replating of Hematopoietic Cells

(A) Experimental design. Murine bone marrow cells were transduced with retroviral vectors expressing mCherry alone (MIC), or mCherry along with *GLIS2*, or *CBFA2T3-GLIS2*. Transduced cells were purified by sorting mCherry-positive cells and plated onto methylcellulose containing IL3, IL6, SCF, and EPO. Colonies were counted after 7 days of growth and replated serially.

(B) Semiquantitative RT-PCR of GLIS2 utilizing cells harvested from first round of plating. *GLIS2* primers are specific for the 3′ half of the transcript and thus pick up both full-length GLIS2 as well as CBFA2T3-GLIS2. Expression in MIC cells was defined as one (1), and data are pooled from two separate experiments with similar results. $p \leq 0.0001$ as determined by one-way ANOVA. Error bars represent mean ± SEM of two independent experiments.

(C) Number of colonies detected at 7 days following each plating. Error bars represent mean ± SEM of two independent experiments.

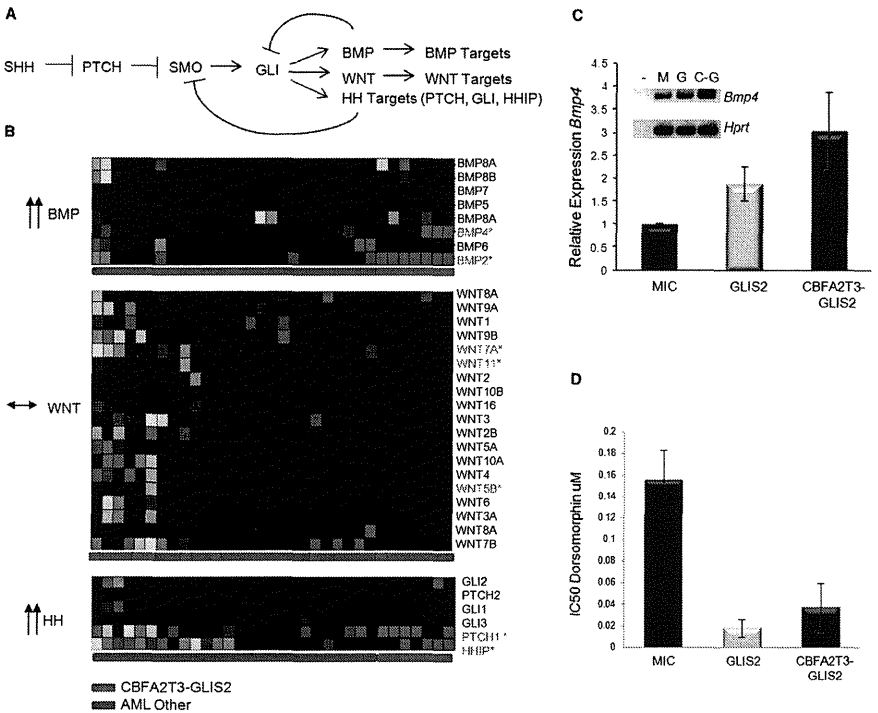

Figure 6. *CBFA2T3-GLIS2* Activates the BMP Pathway

(A) The Hedgehog (HH) signaling pathway. In addition to classic hedgehog targets such as *PTCH* and *HHIP*, *WNT* and *BMP* gene expression have been demonstrated to be affected by the GLI transcription factor in various models (Dahn and Fallon, 2000; Ingham and McMahon, 2001; Vokes et al., 2007).

(B) Gene expression profiles from *CBFA2T3-GLIS2* containing AMKL cases and other AML subtypes were evaluated for expression levels of *BMP*, *WNT*, and *HH* target genes. *CBFA2T3-GLIS2*-negative AMKL cases are not shown in this analysis. Significantly upregulated probe sets (FDR less than 0.05) are designated with red font: BMP2 FDR 1.06 × 10–17, BMP4 FDR 0.015976, PTCH1 FDR 2.05 × 10–6, and HHIP FDR 0.0038.

(C) Murine bone marrow cells were transduced with retroviral vectors carrying mCherry alone (MIC), mCherry plus *GLIS2*, or *CBFA2T3-GLIS2*. mCherry-positive cells were sorted and plated in methylcellulose containing IL3, IL6, SCF, and EPO. Following 1 week of growth, RNA was isolated, reverse transcribed, and amplified with *Bmp4* or *Hprt*-specific primers. Error bars represent mean ± SEM of four independent experiments. A representative gel is shown (–, neg; M, MIC; G, *GLIS2*; C-G, *CBFA2T3-GLIS2*). p = 0.047 as determined by one-way ANOVA.

(D) *GLIS2* and *CBFA2T3-GLIS2* sensitize murine hematopoietic cells to BMP receptor type I inhibition. Colony-formation assays were conducted in the presence or absence of dorsomorphin at the indicated concentrations (Yu et al., 2008). IC_{50} values were calculated as the amount of drug required to inhibit 50% of the colony formation as determined by colony counts. Error bars represent mean ± SEM of two independent experiments. p = 0.036 as determined by one-way ANOVA. See also Figure S4.

biological differences between pediatric and adult AMKL. Importantly, each of the detected chimeric transcripts is predicted to encode a fusion protein that would alter signaling pathways known to play a role in normal hematopoiesis, suggesting that these lesions are "driver" mutations that directly contribute to the development of leukemia. In addition to these somatic

(D) Colony morphology detected in *GLIS2* and *CBFA2T3-GLIS2*-modified cells from the second plating and beyond. a, CFU-Meg; b, CFU-GM. Scale bars, 500 μm. Representative cytospins and morphology of each colony type are shown. c, CFU-Meg; d, CFU-GM. Scale bars, 50 μm.

(E) Cells harvested from colony-forming assays after three or more replatings were subjected to flow cytometry. Cells were negative for acetylcholinesterase (data not shown).

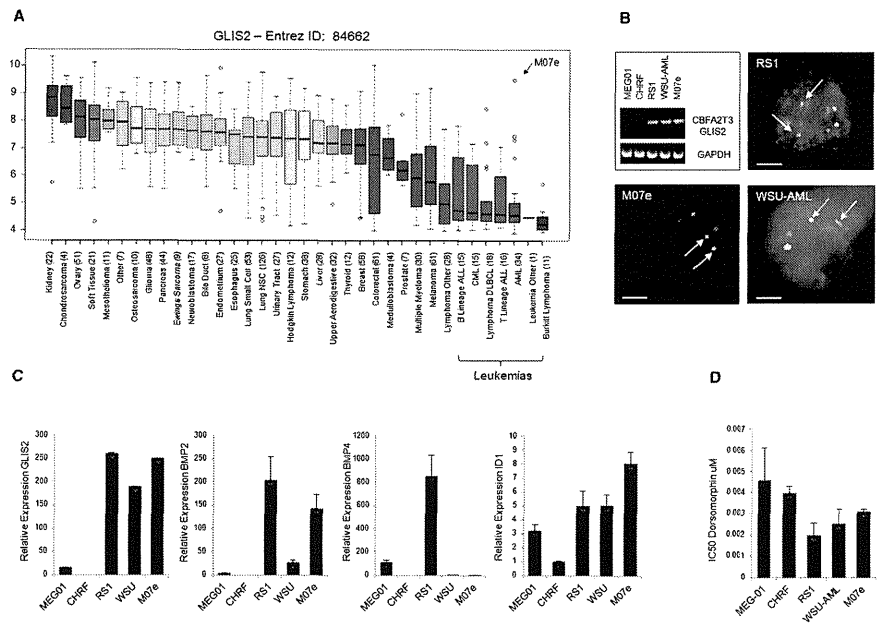

Figure 7. *CBFA2T3-GLIS2* Is Present in AMKL Cell Lines

(A) *GLIS2* expression as determined by gene expression arrays in 991 human cancer cell lines. Log_2-transformed expression levels are shown. Data were obtained from the Broad-Novartis Cancer Cell Line Encyclopedia (http://www.broadinstitute.org/ccle/home). A total of 34 AML cell lines are included; the extreme outlier of this subtype, M07e, is indicated. The *GLIS2* probe set recognizes the end of the transcript and thus does not distinguish between wild-type *GLIS2* and *CBFA2T3-GLIS2*. Median values are indicated by the band within the box plots; the ends of the whiskers indicate upper and lower adjacent values. Outliers are denoted by open circles.

(B) RT-PCR on five AMKL cell lines: MEG-01, CHRF-288-11, RS-1, WSU-AML, and M07e. The three cell lines carrying *CBFA2T3-GLIS2* were validated by FISH. Scale bars, 10 μm.

(C) Real-time semiquantitative RT-PCR of *GLIS2*, *BMP2*, *BMP4*, and *ID1* on the five AMKL cell lines. Expression levels relative to β-actin are shown. CHRF-288-11 expression levels were set to one (1) for comparison across cell lines. Error bars represent mean ± SEM of two independent experiments.

(D) Dorsomorphin sensitivity in the cell lines as determined by MTT assay. Error bars represent mean ± SEM of two independent experiments. For cell line information and MTT assay, please see Supplemental Experimental Procedures.

structural alterations, a variety of other somatic mutations were detected, including activating mutations in kinase signaling pathways in 21.6% of cases (*JAK kinase family members and MPL*), inactivating mutations in *GATA1* in 9.8% of cases, and amplification of chromosome 21 in the DSCR that includes genes known to play a role in AML such as *RUNX1*, *ETS2*, and *ERG* in 50% of the cases. How these mutations interact to not only induce overt leukemia but also to influence therapeutic responses remains to be determined.

As part of the St. Jude Children's Research Hospital-Washington University Pediatric Cancer Genome Project, we have sequenced 260 cases of pediatric cancers across multiple tumor types (Downing et al., 2012). The CBFA2T3-GLIS2 fusion was limited to AMKL cases. This specificity may exist for several reasons. The N-terminal portion of the fusion, CBFA2T3, is primarily expressed in the hematopoietic compartment, leading one to predict that expression of the inversion product, if it were to occur, would primarily be limited to hematopoietic cells. Although we do not know the exact target cell of transformation, induction of BMP4 signaling in human CD34+ progenitors has been demonstrated to increase the percentage of megakaryocyte and erythroid colonies in vitro (Fuchs et al., 2002; Jeanpierre et al., 2008). Thus, enhanced BMP signaling as a result of the expression of the inv(16)-encoded CBFA2T3-GLIS2 may directly contribute to the megakaryocytic differentiation of the leukemia cells.

The inv(16)-encoded *CBFA2T3-GLIS2* chimeric gene induced aberrant high-level expression of the DNA-binding domain of

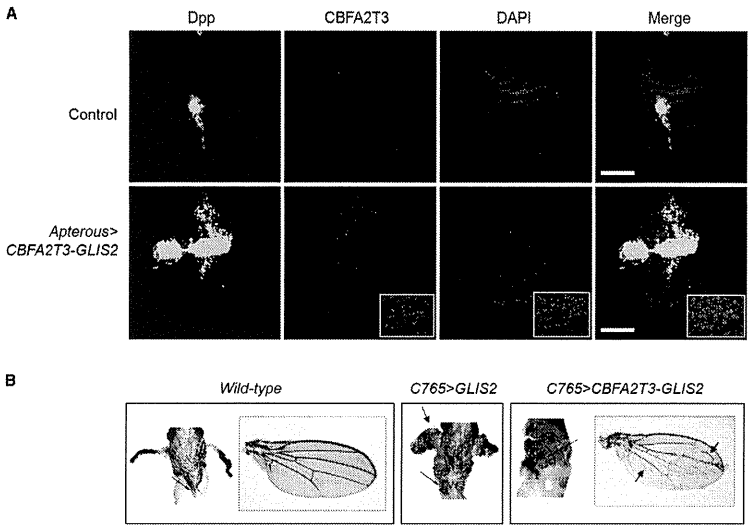

Figure 8. Transgenic *CBFA2T3-GLIS2 Drosophila* Ectopically Expresses Dpp

(A) *CBFA2T3-GLIS2* was expressed under control of *Apterous-Gal4* (strong epithelial dorsal driver). *dpp-lacZ* serves as a reporter for *dpp* induction. Wing imaginal discs were isolated at the late third instar, stained for β-gal as a readout for dpp (green), CBFA2T3 (red), and DAPI (blue), followed by immunofluorescence analysis. Nuclear localization of CBFA2T3-GLIS2 can be seen by the pink signal (inset). Scale bars, 100 μm.

(B) *CBFA2T3-GLIS2* was expressed under control of C765, a weak epithelial driver. Pharate adults were dissected from pupal casings and imaged. Arrows indicate ectopic notum, broadened and shortened legs. No *C765 > GLIS2 Drosophila* matured to adulthood. Arrows indicate ectopic veins in wings of rare *C765 > CBFA2T3-GLIS2* escapers.

See also Figure S5.

GLIS2 in hematopoietic cells, along with the disruption of one allele of *CBFA2T3*, a gene whose encoded protein has been shown to play a role in maintaining normal hematopoietic stem cell quiescence (Chyla et al., 2008). GLIS2 is a distant member of the GLI superfamily of transcriptional factors that function as critical transcriptional targets of the SHH signaling pathway (Hui and Angers, 2011). Although alterations in the SHH pathway have been directly implicated in a range of cancers (Barakat et al., 2010), the role of SHH signaling in normal hematopoiesis and leukemia remains poorly defined (Lim and Matsui, 2010). Our data suggest that aberrant expression of GLIS2 results in upregulation of the classic SHH-negative feedback inhibitors PTCH and HHIP, coupled with a marked increase in the expression of BMP 2 and 4, resulting in enhanced BMP signaling. These results indicate that CBFA2T3-GLIS2 functions, in part, as a gain-of-function GLIS2 allele. The exact mechanisms by which GLIS2 induced the upregulation of BMP2/BMP4 remains incompletely defined, although our data suggest that a direct transcription effect of GLIS2 on the BMP4 promoter is likely, although an indirect mechanism may also contribute.

Interestingly, BMP4 has been shown to expand and maintain human cord blood hematopoietic stem cells in vitro both directly, as well as indirectly via SHH signaling (Bhardwaj et al., 2001; Bhatia et al., 1999). Furthermore, *ID1*, a downstream BMP target previously implicated in leukemogenesis, was found to be upregulated in *CBFA2T3-GLIS2*-modified hematopoietic cells, demonstrating that this pathway is activated (Wang et al., 2011). Consistent with these findings, we demonstrated that activation of BMP signaling contributed to the marked increase in the replating capacity of myeloid/erythroid-committed progenitors. Accordingly, we found that murine hematopoietic cells carrying either full-length *GLIS2*, or *CBFA2T3-GLIS2*, demonstrated an increased sensitivity to BMP inhibition, suggesting that upregulation of this pathway contributes to the observed phenotype. In addition, BMP4 signaling has been shown to induce the differentiation of human CD34+ progenitors into megakaryocytes (Jeanpierre et al., 2008), suggesting that the upregulation of this pathway is also contributing to the megakaryocyte differentiation phenotype of these leukemias. Finally, BMP4, like thrombopoietin, appears to exert its effects on human megakaryopoiesis in part through the JAK/STAT pathways (Jeanpierre et al., 2008). Interestingly, functional pathway analysis of gene expression profiles in *CBFA2T3-GLIS2*-positive AMKL samples identified genes in the Jak-STAT signaling pathway to be significantly upregulated (p = 0.0038; FDR 0.022978; Figure S4). Combined with the identification in some cases of activating mutations in either JAK family members or MPL in *CBFA2T3-GLIS2*-expressing leukemias, our data suggest that these lesions likely cooperate in leukemogenesis.

Taken together, these data define a poor prognostic subgroup of pediatric AMKL patients that are characterized by the inv(16)(p13.3q24.3)-encoded CBFA2T3-GLIS2 fusion protein. Expression of *CBFA2T3-GLIS2* induces an enhanced replating capacity of lineage-committed myeloid progenitors, along with megakaryocytic differentiation, in part through enhanced BMP2/BMP4 signaling. Whether altered SHH and CBFA2T3-induced signaling also contributes to leukemogenesis remains to be determined. Nevertheless, the presented data raise the important possibility that inhibition of the BMP pathway may have a therapeutic benefit in this aggressive form of pediatric AML.

EXPERIMENTAL PROCEDURES

Patients and Samples

Paired-end transcriptome sequencing on diagnostic leukemic blasts was performed on 14 pediatric non-DS-AMKL cases using the Illumina platform. Four of these cases underwent whole-genome sequencing (WGS) on diagnostic leukemia blasts and matched germline samples. All 14 cases underwent whole-exome sequencing for which 10 had matching germline samples. One additional diagnostic sample with matched germline DNA had whole-exome sequencing done that did not undergo transcriptome sequencing. All 15 of these patients were treated at St Jude Children's Research Hospital from 1990 to 2008. The recurrence cohort consisted of 61 additional cases including 33 pediatric specimens and 28 adult specimens . All samples were obtained with patient or parent/guardian-provided informed consent under protocols approved by the Institutional Review Board at each institution and St. Jude Children's Research Hospital.

Sequencing

RNA and DNA library construction for transcriptome and whole-genome DNA sequencing, respectively, has been described previously (Mardis et al., 2009; Zhang et al., 2012). Analysis of WGS data and whole-exome sequencing data that include mapping, coverage and quality assessment, single-nucleotide variant (SNV)/Indel detection, tier annotation for sequence mutations, prediction of deleterious effects of missense mutations, and identification of loss of heterozygosity was described previously (Zhang et al., 2012). Please see Supplemental Experimental Procedures for details.

Recurrency Screening for Sequence Variations and Fusions

We performed recurrence screening on a cohort of 61 AMKL samples. All 61 were screened by RT-PCR (see Supplemental Experimental Procedures for primers and conditions) for *CBFA2T3-GLIS2*, *GATA2-HOXA9*, *MN1-FLI1*, *NIPBL-HOXB9*, and *NUP98-KDM5A*. Whole-genome-amplified DNA (QIAGEN) from 38 cases underwent PCR and Sanger sequencing by Beckman Coulter Genomics for *JAK1*, *JAK2*, *JAK3*, and *MPL* mutations. In 8 of 38 cases, a paired matched germline was available. Putative SNVs and indel variants were detected by SNPdetector (Zhang et al., 2005).

Overall Survival Probabilities

Outcome data were available for 40 pediatric patients tested for *CBFA2T3-GLIS2*. *CBFA2T3-GLIS2* was found in 13 patients. Overall survival was defined as the date of diagnosis or study enrollment to the date of death with surviving patients censored at the date of last follow-up. Survival curves were estimated using the Kaplan-Meier method and compared using the exact log rank test based on 10,000 permutations.

Affymetrix SNP Array

Affymetrix SNP 6.0 array genotyping was performed for 14 of 15 AMKL cases in the discovery cohort, and array normalization and DNA copy number alterations were identified as previously described (Lin et al., 2004; Mullighan et al., 2007; Olshen et al., 2004; Pounds et al., 2009). To differentiate inherited copy number alterations from somatic events in leukemia blasts from patients lacking matched normal DNA, identified putative variants were filtered using public copy number polymorphism databases and a St. Jude database of SNP array data from several hundred samples (Iafrate et al., 2004; McCarroll et al., 2008).

Gene Expression Profiling

Gene expression profiling was performed using Affymetrix Human Exon 1.0 ST Arrays (Affymetrix) according to manufacturer's instructions. This cohort comprised 39 pediatric AML samples including AMKL (n = 14), *AML1-ETO* (n = 4), *CBFB-MYH11* (n = 2), *MLL* rearranged (n = 3), *PML-RARA* (n = 2), *NUP98-NSD1* (n = 2), *HLXB9-ETV6* (n = 1), and AML cases lacking chimeric genes (n = 11). Please see Supplemental Experimental Procedures for further details.

FISH

Dual-color FISH was performed on archived bone marrow cells and cell lines as described previously by Mullighan et al. (2007). Probes were derived from bacterial artificial chromosome (BAC) clones (Invitrogen). BACs used were RP11-830F9 (*CBFA2T3*), CTD-25555M20 (*GLIS2*), RP11-345E21 (*MN1*), and CTD-2542E23 (*FLI1*). BAC clone identity was verified by T7 and SP6 BAC-end sequencing and by hybridization of fluorescently labeled BAC DNA with normal human metaphase preparations.

Cloning of CBFA2T3-GLIS2 and GLIS2

Total RNA was extracted from leukemia blasts using RNeasy (QIAGEN) and reverse transcribed using Superscript III (Invitrogen) as per manufacturer's instructions. The coding region of *CBFA2T3-GLIS2* was PCR amplified from patient M712 and M707 using primers CBFA2T3_119F and GLIS2_1685R (see Supplemental Experimental Procedures for primers and conditions). *GLIS2* was PCR amplified from cDNA using primers GLIS2_21F and GLIS2_1685R (see Supplemental Experimental Procedures for primers and conditions). PCR products were subcloned into the pGEM-T Easy Vector (Promega) and sequenced. Clones containing the correct sequence were then subcloned into the MIC retroviral backbone (Volanakis et al., 2009).

Murine Bone Marrow Transduction and Colony-Forming Assays

All experiments involving mice were reviewed and approved by the Institutional Animal Care and Use Committee. Bone marrow from 4- to 6-week-old female C57/BL6 mice was harvested and cultured in the presence of recombinant murine SCF (rmSCF), IL3 (rmIL3), and IL6 (rmIL6) (Peprotech; all 50 ng/ml) for 24 hr prior to transduction on RetroNectin (Takara Bio)-coated plates. Ecotropic envelope-pseudotyped retroviral supernatant was produced by transient transfection of 293T cells as previously described by Soneoka et al. (1995). Forty-eight hours following transduction, cells were harvested, sorted for mCherry expression, and plated on methylcellulose containing IL3, IL6, SCF, and EPO (Stem Cell Technologies, Vancouver, British Columbia, Canada) as per manufacturer's instructions. Colonies were counted after 7 days of growth at 37°C, harvested, and replated. In a subset of experiments, dorsomorphin (Sigma-Aldrich) was added to the methylcellulose at the indicated concentrations.

Flow Cytometry

Cells were resuspended in PBS and preincubated with anti-CD16/CD32 Fc-block (BD PharMingen) if staining did not include conjugated anti-murine CD16/32. Aliquots were stained for 15 min at 4°C with conjugated antibodies. Cells were washed and resuspended in DAPI containing solution (1 μg/ml DAPI in PBS) for subsequent analysis using FACS LSR II D (BD Biosciences). For a list of antibodies used, please see Supplemental Experimental Procedures.

Luciferase Assays

The human BMP4 promoter-driven luciferase construct pSLA4.1EX (Van den Wijngaard et al., 1999) was kindly provided by E. Joop van Zoelen, Nijmegen, The Netherlands. The murine BMP response element (pBRE) (Korchynskyi and ten Dijke, 2002) was kindly provided by Peter ten Dijke, Leiden, The Netherlands. The 8 × 3′ Gli-BS luciferase reporter (pGli-BS) (Sasaki et al., 1997) has been previously described. TOPFlash and FOPFlash (Korinek et al., 1997) constructs were obtained from Addgene. For details on luciferase reporter assays, please see Supplemental Experimental Procedures.

Cancer Cell
CBFA2T3-GLIS2 Defines an Aggressive Type of AMKL

ELISA

BMP4 protein levels in the supernatants from transduced murine hematopoietic cells were determined by ELISA. Briefly, mCherry-positive bone marrow cells transduced with empty (MIC), GLIS2, or CBFA2T3-GLIS2-containing retroviruses were placed in media containing IL3, IL6, and SCF for 48 hr, and supernatant was then harvested and the level of murine BMP4 determined using an ELISA kit purchased from TSZELISA (http://www.tszelisa.com). Measurements were done according to manufacturer's instructions.

Transgenic *Drosophila*

CBFA2T3-GLIS2 and *GLIS2* cDNAs were subcloned into the *pUAS-attB* plasmid (Bischof et al., 2007). Transgenic UAS-*CBFA2T3-GLIS2* and UAS-*GLIS2* flies were generated using site-specific ϕC31 integration system (Bischof et al., 2007). Embryo injections were performed by Best Gene. UAS constructs were targeted to chromosome 2R-51D in order to avoid differential positional effects on transgene expression. For wing imaginal disc staining, relevant crosses were performed to generate flies carrying all three transgenes: *Apterous-Gal4* (a strong epithelial dorsal compartment-specific GAL4 driver), UAS-*CBFA2T3-GLIS2*, and a *dpp-lacZ* enhancer trap reporter. Gal4 driver and *dpp-lacZ* reporter stocks were obtained from the Bloomington Stock Center. Wing imaginal discs were dissected from wandering third-instar larvae, fixed, and immunostained using anti-β-gal (Promega; Z378), anti-CBFA2T3 (Abcam; ab33072), and DAPI (Invitrogen; D3571) as previously described by Carroll et al. (2012). To assess the phenotypic effects of *CBFA2T3-GLIS2* and *GLIS2*, UAS transgenes were expressed under control of the epithelial driver *C765-Gal4*, and progeny was observed. Pharate adults were dissected from pupal casings and imaged.

ACCESSION NUMBERS

The sequence data and SNP microarray data have been deposited in the dbGaP database (http://www.ncbi.nlm.nih.gov/gap) under the accession number phs000413.v1.p1. Affymetrix gene expression data have been deposited in the NCBI Gene Expression Omnibus (http://www.ncbi.nlm.nih.gov/geo/) under GSE35203.

SUPPLEMENTAL INFORMATION

Supplemental Information includes five figures, seven tables, and Supplemental Experimental Procedures and can be found with this article online at http://dx.doi.org/10.1016/j.ccr.2012.10.007.

ACKNOWLEDGMENTS

The authors would like to specifically thank Joy Nakitandwe for critical input and discussions, Susana Raimondi for review of cytogenetics, Matt Stine for assistance with data deposition, Bill Pappas and Scott Malone for support of the information technology infrastructure, and the staff of Tissue Resources Laboratory, Flow Cytometry and Cell Sorting Core, the Hartwell Center for Biotechnology and Bioinformatics of St Jude Children's Research Hospital, and Emily Dolezale for assistance in sample procurement at Memorial Sloan Kettering Cancer Center. This work was supported by grants from the National Institutes of Health (Cancer Center Support Grant P30 CA021765), the Eric Trump Foundation, a Leukemia & Lymphoma Society Specialized Center of Research Grant LLS7015, and the American Lebanese Syrian Associated Charities (ALSAC) of St Jude Children's Research Hospital.

Received: June 21, 2012
Revised: September 5, 2012
Accepted: October 17, 2012
Published: November 12, 2012

REFERENCES

Argiropoulos, B., and Humphries, R.K. (2007). Hox genes in hematopoiesis and leukemogenesis. Oncogene *26*, 6766–6776.

Athale, U.H., Razzouk, B.I., Raimondi, S.C., Tong, X., Behm, F.G., Head, D.R., Srivastava, D.K., Rubnitz, J.E., Bowman, L., Pui, C.H., and Ribeiro, R.C. (2001). Biology and outcome of childhood acute megakaryoblastic leukemia: a single institution's experience. Blood *97*, 3727–3732.

Attanasio, M., Uhlenhaut, N.H., Sousa, V.H., O'Toole, J.F., Otto, E., Anlag, K., Klugmann, C., Treier, A.C., Helou, J., Sayer, J.A., et al. (2007). Loss of GLIS2 causes nephronophthisis in humans and mice by increased apoptosis and fibrosis. Nat. Genet. *39*, 1018–1024.

Barakat, M.T., Humke, E.W., and Scott, M.P. (2010). Learning from Jekyll to control Hyde: Hedgehog signaling in development and cancer. Trends Mol. Med. *16*, 337–348.

Barnard, D.R., Alonzo, T.A., Gerbing, R.B., Lange, B., and Woods, W.G.; *Children's Oncology Group. (2007). Comparison of childhood myelodysplastic* syndrome, AML FAB M6 or M7, CCG 2891: report from the Children's Oncology Group. Pediatr. Blood Cancer *49*, 17–22.

Barretina, J., Caponigro, G., Stransky, N., Venkatesan, K., Margolin, A.A., Kim, S., Wilson, C.J., Lehár, J., Kryukov, G.V., Sonkin, D., et al. (2012). The Cancer Cell Line Encyclopedia enables predictive modelling of anticancer drug sensitivity. Nature *483*, 603–607.

Bhardwaj, G., Murdoch, B., Wu, D., Baker, D.P., Williams, K.P., Chadwick, K., Ling, L.E., Karanu, F.N., and Bhatia, M. (2001). Sonic hedgehog induces the proliferation of primitive human hematopoietic cells via BMP regulation. Nat. Immunol. *2*, 172–180.

Bhatia, M., Bonnet, D., Wu, D., Murdoch, B., Wrana, J., Gallacher, L., and Dick, J.E. (1999). Bone morphogenetic proteins regulate the developmental program of human hematopoietic stem cells. J. Exp. Med. *189*, 1139–1148.

Bischof, J., Maeda, R.K., Hediger, M., Karch, F., and Basler, K. (2007). An optimized transgenesis system for *Drosophila* using germ-line-specific phiC31 integrases. Proc. Natl. Acad. Sci. USA *104*, 3312–3317.

Buijs, A., van Rompaey, L., Molijn, A.C., Davis, J.N., Vertegaal, A.C., Potter, M.D., Adams, C., van Baal, S., Zwarthoff, E.C., Roussel, M.F., and Grosveld, G.C. (2000). The MN1-TEL fusion protein, encoded by the translocation (12;22)(p13;q11) in myeloid leukemia, is a transcription factor with transforming activity. Mol. Cell. Biol. *20*, 9281–9293.

Carroll, A., Civin, C., Schneider, N., Dahl, G., Pappo, A., Bowman, P., Emami, A., Gross, S., Alvarado, C., Phillips, C., *et al. (1991). The t(1;22) (p13;q13)* is nonrandom and restricted to infants with acute megakaryoblastic leukemia: a Pediatric Oncology Group Study. Blood *78*, 748–752.

Carroll, C.E., Marada, S., Stewart, D.P., Ouyang, J.X., and Ogden, S.K. (2012). The extracellular loops of Smoothened play a regulatory role in control of Hedgehog pathway activation. Development *139*, 612–621.

Chyla, B.J., Moreno-Miralles, I., Steapleton, M.A., Thompson, M.A., Bhaskara, S., Engel, M., and Hiebert, S.W. (2008). Deletion of Mtg16, a target of t(16;21), alters hematopoietic progenitor cell proliferation and lineage allocation. Mol. Cell. Biol. *28*, 6234–6247.

Creutzig, U., Reinhardt, D., Diekamp, S., Dworzak, M., Stary, J., and Zimmermann, M. (2005). AML patients with Down syndrome have a high cure rate with AML-BFM therapy with reduced dose intensity. Leukemia *19*, 1355–1360.

Dahn, R.D., and Fallon, J.F. (2000). Interdigital regulation of digit identity and homeotic transformation by modulated BMP signaling. Science *289*, 438–441.

Downing, J.R., Wilson, R.K., Zhang, J., Mardis, E.R., Pui, C.-H., Ding, L., Ley, T.J., and Evans, W.E. (2012). The Pediatric Cancer Genome Project. Nat. Genet. *44*, 619–622.

Fuchs, O., Simakova, O., Klener, P., Cmejlova, J., Zivny, J., Zavadil, J., and Stopka, T. (2002). Inhibition of Smad5 in human hematopoietic progenitors blocks erythroid differentiation induced by BMP4. Blood Cells Mol. Dis. *28*, 221–233.

Gamou, T., Kitamura, E., Hosoda, F., Shimizu, K., Shinohara, K., Hayashi, Y., Nagase, T., Yokoyama, Y., and Ohki, M. (1998). The partner gene of AML1 in t(16;21) myeloid malignancies is a novel member of the MTG8(ETO) family. Blood *91*, 4028–4037.

Grieder, N.C., Morata, G., Affolter, M., and Gehring, W.J. (2009). Spalt major controls the development of the notum and of wing hinge primordia of the *Drosophila melanogaster* wing imaginal disc. Dev. Biol. *329*, 315–326.

Heuser, M., Yun, H., Berg, T., Yung, E., Argiropoulos, B., Kuchenbauer, F., Park, G., Hamwi, I., Palmqvist, L., Lai, C.K., et al. (2011). Cell of origin in AML: susceptibility to MN1-induced transformation is regulated by the MEIS1/AbdB-like HOX protein complex. Cancer Cell *20*, 39–52.

Higuchi, M., O'Brien, D., Kumaravelu, P., Lenny, N., Yeoh, E.J., and Downing, J.R. (2002). Expression of a conditional AML1-ETO oncogene bypasses embryonic lethality and establishes a murine model of human t(8;21) acute myeloid leukemia. Cancer Cell *1*, 63–74.

Hui, C.C., and Angers, S. (2011). Gli proteins in development and disease. Annu. Rev. Cell Dev. Biol. *27*, 513–537.

Iafrate, A.J., Feuk, L., Rivera, M.N., Listewnik, M.L., Donahoe, P.K., Qi, Y., Scherer, S.W., and Lee, C. (2004). Detection of large-scale variation in the human genome. Nat. Genet. *36*, 949–951.

Ingham, P.W., and McMahon, A.P. (2001). Hedgehog signaling in animal development: paradigms and principles. Genes Dev. *15*, 3059–3087.

Jeanpierre, S., Nicolini, F.E., Kaniewski, B., Dumontet, C., Rimokh, R., Puisieux, A., and Maguer-Satta, V. (2008). BMP4 regulation of human megakaryocytic differentiation is involved in thrombopoietin signaling. Blood *112*, 3154–3163.

Kawada, H., Ito, T., Pharr, P.N., Spyropoulos, D.D., Watson, D.K., and Ogawa, M. (2001). Defective megakaryopoiesis and abnormal erythroid development in Fli-1 gene-targeted mice. Int. J. Hematol. *73*, 463–468.

Kim, Y.S., Kang, H.S., and Jetten, A.M. (2007). The Krüppel-like zinc finger protein Glis2 functions as a negative modulator of the Wnt/beta-catenin signaling pathway. FEBS Lett. *581*, 858–864.

Korchynskyi, O., and ten Dijke, P. (2002). Identification and functional characterization of distinct critically important bone morphogenetic protein-specific response elements in the Id1 promoter. J. Biol. Chem. *277*, 4883–4891.

Korinek, V., Barker, N., Morin, P.J., van Wichen, D., de Weger, R., Kinzler, K.W., Vogelstein, B., and Clevers, H. (1997). Constitutive transcriptional activation by a beta-catenin-Tcf complex in APC-/- colon carcinoma. Science *275*, 1784–1787.

Krzywinski, M., Schein, J., Birol, I., Connors, J., Gascoyne, R., Horsman, D., Jones, S.J., and Marra, M.A. (2009). Circos: an information aesthetic for comparative genomics. Genome Res. *19*, 1639–1645.

Lamar, E., Kintner, C., and Goulding, M. (2001). Identification of NKL, a novel Gli-Kruppel zinc-finger protein that promotes neuronal differentiation. Development *128*, 1335–1346.

Lim, Y., and Matsui, W. (2010). Hedgehog signaling in hematopoiesis. Crit. Rev. Eukaryot. Gene Expr. *20*, 129–139.

Lin, M., Wei, L.J., Sellers, W.R., Lieberfarb, M., Wong, W.H., and Li, C. (2004). dChipSNP: significance curve and clustering of SNP-array-based loss-of-heterozygosity data. Bioinformatics *20*, 1233–1240.

Lion, T., Haas, O.A., Harbott, J., Bannier, E., Ritterbach, J., Jankovic, M., Fink, F.M., Stojimirovic, A., Herrmann, J., Riehm, H.J., et al. (1992). The translocation t(1;22)(p13;q13) is a nonrandom marker specifically associated with acute megakaryocytic leukemia in young children. Blood *79*, 3325–3330.

Ma, Z., Morris, S.W., Valentine, V., Li, M., Herbrick, J.A., Cui, X., Bouman, D., Li, Y., Mehta, P.K., Nizetic, D., et al. (2001). Fusion of two novel genes, RBM15 and MKL1, in the t(1;22)(p13;q13) of acute megakaryoblastic leukemia. Nat. Genet. *28*, 220–221.

Malinge, S., Ragu, C., Della-Valle, V., Pisani, D., Constantinescu, S.N., Perez, C., Villeval, J.L., Reinhardt, D., Landman-Parker, J., Michaux, L., et al. (2008). Activating mutations in human acute megakaryoblastic leukemia. Blood *112*, 4220–4226.

Mardis, E.R., Ding, L., Dooling, D.J., Larson, D.E., McLellan, M.D., Chen, K., Koboldt, D.C., Fulton, R.S., Delehaunty, K.D., McGrath, S.D., et al. (2009). Recurring mutations found by sequencing an acute myeloid leukemia genome. N. Engl. J. Med. *361*, 1058–1066.

McCarroll, S.A., Kuruvilla, F.G., Korn, J.M., Cawley, S., Nemesh, J., Wysoker, A., Shapero, M.H., de Bakker, P.I., Maller, J.B., Kirby, A., et al. (2008). Integrated detection and population-genetic analysis of SNPs and copy number variation. Nat. Genet. *40*, 1166–1174.

Mercher, T., Coniat, M.B., Monni, R., Mauchauffe, M., Nguyen Khac, F., Gressin, L., Mugneret, F., Leblanc, T., Dastugue, N., Berger, R., and Bernard, O.A. (2001). Involvement of a human gene related to the *Drosophila* spen gene in the recurrent t(1;22) translocation of acute megakaryocytic leukemia. Proc. Natl. Acad. Sci. USA *98*, 5776–5779.

Mullighan, C.G., Goorha, S., Radtke, I., Miller, C.B., Coustan-Smith, E., Dalton, J.D., Girtman, K., Mathew, S., Ma, J., Pounds, S.B., et al. (2007). Genome-wide analysis of genetic alterations in acute lymphoblastic leukaemia. Nature *446*, 758–764.

Oki, Y., Kantarjian, H.M., Zhou, X., Cortes, J., Faderl, S., Verstovsek, S., O'Brien, S., Koller, C., Beran, M., Bekele, B.N., et al. (2006). Adult acute megakaryocytic leukemia: an analysis of 37 patients treated at M.D. Anderson Cancer Center. Blood *107*, 880–884.

Olshen, A.B., Venkatraman, E.S., Lucito, R., and Wigler, M. (2004). Circular binary segmentation for the analysis of array-based DNA copy number data. Biostatistics *5*, 557–572.

Pounds, S., Cheng, C., Mullighan, C., Raimondi, S.C., Shurtleff, S., and Downing, J.R. (2009). Reference alignment of SNP microarray signals for copy number analysis of tumors. Bioinformatics *25*, 315–321.

Radtke, I., Mullighan, C.G., Ishii, M., Su, X., Cheng, J., Ma, J., Ganti, R., Cai, Z., Goorha, S., Pounds, S.B., et al. (2009). Genomic analysis reveals few genetic alterations in pediatric acute myeloid leukemia. Proc. Natl. Acad. Sci. USA *106*, 12944–12949.

Sander, V., Eivers, E., Choi, R.H., and De Robertis, E.M. (2010). *Drosophila* Smad2 opposes Mad signaling during wing vein development. PLoS One *5*, e10383.

Sasaki, H., Hui, C., Nakafuku, M., and Kondoh, H. (1997). A binding site for Gli proteins is essential for HNF-3beta floor plate enhancer activity in transgenics and can respond to Shh in vitro. Development *124*, 1313–1322.

Söderberg, S.S., Karlsson, G., and Karlsson, S. (2009). Complex and context dependent regulation of hematopoiesis by TGF-beta superfamily signaling. Ann. N Y Acad. Sci. *1176*, 55–69.

Soneoka, Y., Cannon, P.M., Ramsdale, E.E., Griffiths, J.C., Romano, G., Kingsman, S.M., and Kingsman, A.J. (1995). A transient three-plasmid expression system for the production of high titer retroviral vectors. Nucleic Acids Res. *23*, 628–633.

Tabata, T., and Takei, Y. (2004). Morphogens, their identification and regulation. Development *131*, 703–712.

Tallman, M.S., Neuberg, D., Bennett, J.M., Francois, C.J., Paietta, E., Wiernik, P.H., Dewald, G., Cassileth, P.A., Oken, M.M., and Rowe, J.M. (2000). Acute megakaryocytic leukemia: the Eastern Cooperative Oncology Group experience. Blood *96*, 2405–2411.

Van den Wijngaard, A., Pijpers, M.A., Joosten, P.H., Roelofs, J.M., Van zoelen, E.J., and Olijve, W. (1999). Functional characterization of two promoters in the human bone morphogenetic protein-4 gene. J. Bone Miner. Res. *14*, 1432–1441.

Visvader, J.E., Crossley, M., Hill, J., Orkin, S.H., and Adams, J.M. (1995). The C-terminal zinc finger of GATA-1 or GATA-2 is sufficient to induce megakaryocytic differentiation of an early myeloid cell line. Mol. Cell. Biol. *15*, 634–641.

Vokes, S.A., Ji, H., McCuine, S., Tenzen, T., Giles, S., Zhong, S., Longabaugh, W.J., Davidson, E.H., Wong, W.H., and McMahon, A.P. (2007). Genomic characterization of Gli-activator targets in sonic hedgehog-mediated neural patterning. Development *134*, 1977–1989.

Volanakis, E.J., Williams, R.T., and Sherr, C.J. (2009). Stage-specific Arf tumor *suppression in Notch1-induced T-cell acute lymphoblastic leukemia. Blood* *114*, 4451–4459.

Wang, G.G., Song, J., Wang, Z., Dormann, H.L., Casadio, F., Li, H., Luo, J.L., Patel, D.J., and Allis, C.D. (2009). Haematopoietic malignancies caused by dysregulation of a chromatin-binding PHD finger. Nature *459*, 847–851.

Wang, L., Gural, A., Sun, X.J., Zhao, X., Perna, F., Huang, G., Hatlen, M.A., Vu, L., Liu, F., Xu, H., et al. (2011). The leukemogenicity of AML1-ETO is dependent on site-specific lysine acetylation. Science *333*, 765–769.

Yu, P.B., Hong, C.C., Sachidanandan, C., Babitt, J.L., Deng, D.Y., Hoyng, S.A., Lin, H.Y., Bloch, K.D., and Peterson, R.T. (2008). Dorsomorphin inhibits BMP signals required for embryogenesis and iron metabolism. Nat. Chem. Biol. *4*, 33–41.

Zhang, J., Wheeler, D.A., Yakub, I., Wei, S., Sood, R., Rowe, W., Liu, P.P., Gibbs, R.A., and Buetow, K.H. (2005). SNPdetector: a software tool for sensitive and accurate SNP detection. PLoS Comput. Biol. *1*, e53.

Zhang, J., Ding, L., Holmfeldt, L., Wu, G., Heatley, S.L., Payne-Turner, D., Easton, J., Chen, X., Wang, J., Rusch, M., et al. (2012). The genetic basis of early T-cell precursor acute lymphoblastic leukaemia. Nature *481*, 157–163.

BRIEF REPORT

Thrombosis from a Prothrombin Mutation Conveying Antithrombin Resistance

Yuhri Miyawaki, M.Sc., Atsuo Suzuki, M.Sc., Junko Fujita, B.Sc., Asuka Maki, B.Sc., Eriko Okuyama, B.Sc., Moe Murata, B.Sc., Akira Takagi, Ph.D., Takashi Murate, M.D., Ph.D., Shinji Kunishima, Ph.D., Michio Sakai, M.D., Kohji Okamoto, M.D., Ph.D., Tadashi Matsushita, M.D., Ph.D., Tomoki Naoe, M.D., Ph.D., Hidehiko Saito, M.D., Ph.D., and Tetsuhito Kojima, M.D., Ph.D.

From the Departments of Pathophysiological Laboratory Sciences (Y.M., A.S., J.F., A.M., E.O., M.M., A.T., T. Murate, T.K.) and Hematology–Oncology (T.N.), Nagoya University Graduate School of Medicine, the Department of Medical Technology, Nagoya University School of Health Sciences (A.T., T. Murate, T.K.), the Department of Advanced Diagnosis, Clinical Research Center (S.K.), National Hospital Organization, Nagoya Medical Center (S.K., H.S.), and the Department of Transfusion Medicine, Nagoya University Hospital (T. Matsushita), Nagoya; and the Departments of Pediatrics (M.S.) and Surgery 1 (K.O.), University of Occupational and Environmental Health, Kita-kyushu — all in Japan. Address reprint requests to Dr. Kojima at the Department of Medical Technology, Nagoya University School of Health Sciences, 1-1-20 Daiko-Minami, Higashi-ku, Nagoya 461-8673, Japan, or at kojima@met.nagoya-u.ac.jp.

N Engl J Med 2012;366:2390-6.

SUMMARY

We identified a novel mechanism of hereditary thrombosis associated with antithrombin resistance, with a substitution of arginine for leucine at position 596 (p.Arg596Leu) in the gene encoding prothrombin (called prothrombin Yukuhashi). The mutant prothrombin had moderately lower activity than wild-type prothrombin in clotting assays, but the formation of thrombin–antithrombin complex was substantially impaired. A thrombin-generation assay revealed that the peak activity of the mutant prothrombin was fairly low, but its inactivation was extremely slow in reconstituted plasma. The Leu596 substitution caused a gain-of-function mutation in the prothrombin gene, resulting in resistance to antithrombin and susceptibility to thrombosis.

PATIENTS WITH HEREDITARY THROMBOPHILIA OFTEN PRESENT WITH UNusual clinical episodes of venous thrombosis at a young age and recurrence in atypical vessels, often with a family history of the condition.[1] Genetic studies of hereditary thrombophilia have revealed two types of genetic defects: loss-of-function mutations in the natural anticoagulants antithrombin, protein C, and protein S, along with gain-of-function mutations in procoagulant factors V (factor V Leiden) and II (prothrombin G20210A).[2] To date, numerous genetic defects have been found in families with hereditary thrombophilia, but there may be many undiscovered causative mutations.[3] Here, we describe a case of hereditary thrombosis induced by a novel mechanism of antithrombin resistance, a gain-of-function mutation in the gene encoding the clotting factor prothrombin (prothrombin Yukuhashi).

CASE REPORT

The proband was a 17-year-old Japanese girl who had a first episode of deep-vein thrombosis at the age of 11 years and had since been treated with warfarin. Her family originated in Yukuhashi in the northern part of the Kyushu islands. At least nine of her family members had had one or more episodes of deep-vein thrombosis (Fig. 1A), including two with pulmonary embolism and three who died from thrombosis. Five family members, including the proband, had had juvenile thrombosis, with two reporting episodes during early childhood. Previous studies did not identify any known causes of hereditary thrombophilia in this family.[4]

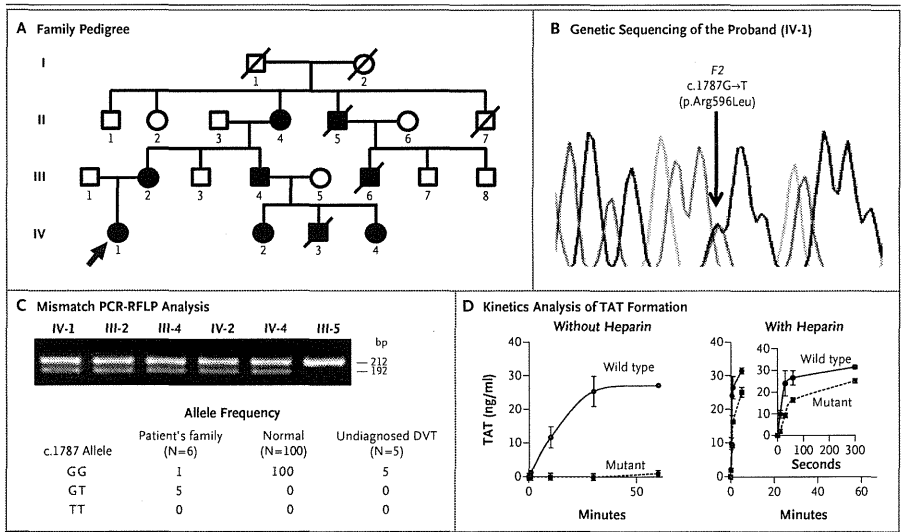

Figure 1. Prothrombin Genotype of a Family with Hereditary Thrombophilia.

Panel A shows the family pedigree. The proband (IV-1) is indicated by an arrow. Solid symbols represent affected family members, open symbols unaffected family members, and slashed symbols deceased family members. Circles represent female family members, and squares male family members. Panel B shows the sequence of the prothrombin gene around the site of the mutation in exon 14. A G→T transversion at nucleotide 1787 of the coding sequence (c.1787G→T) has occurred in the gene encoding the clotting factor prothrombin Yukuhashi, resulting in an amino acid substitution of leucine for arginine at position 596 (p.Arg596Leu). The proband is heterozygous for the mutation (arrow). Panel C shows a restriction-fragment–length polymorphism (RFLP) analysis of the mismatch polymerase-chain-reaction (PCR) product of exon 14 of the prothrombin gene digested by PstI endonuclease. The wild-type prothrombin gene has an undigested fragment of 212 bp. The mutation in the prothrombin Yukuhashi gene creates a PstI site, resulting in a digestion fragment of 192 bp. The table shows allele frequencies at c.1787 of the prothrombin gene in 6 family members, in 100 Japanese persons with a normal phenotype, and in 5 persons with previously undiagnosed deep-vein thrombosis (DVT). Panel D shows the kinetics analysis of thrombin–antithrombin complex (TAT) formation of recombinant wild-type and p.Arg596Leu mutant prothrombins, in the presence and absence of heparin. TAT levels were measured with the use of an enzyme-linked immunosorbent assay and various incubation times for antithrombin and recombinant thrombins; the latter are forms of recombinant prothrombins activated by factor Xa.

METHODS

DNA ANALYSIS

We amplified all 14 exons, including the exon–intron boundaries and the 3′ untranslated region, of the prothrombin gene by means of polymerase chain reaction (PCR), using gene-specific primers (see Table S1 in the Supplementary Appendix, available with the full text of this article at NEJM.org). The amplicons were sequenced as described previously.[5] To detect the mutation, we performed PCR–restriction-fragment–length polymorphism (RFLP) analysis, using a mismatched lower primer (5′-TGTAGAAGCCATATTTCCCcTgC-3′, with base substitutions at c and g) and introducing a PstI site into the amplicon from a mutant allele. Genomic DNA was isolated from peripheral leukocytes by phenol extraction.[6]

RECOMBINANT PROTHROMBINS

We used a PCR assay to prepare full-length human prothrombin complementary DNA (cDNA) obtained from a human liver cDNA library (Clontech) and cloned this into pcDNA™3.1(+) (Invitrogen) to obtain a wild-type human prothrombin expression vector. Subsequently, we prepared a mutant prothrombin expression vector by means of overlap extension PCR,[7] using two primers: 5′-TGAAGGCTGTGACCtGGATGGGAAA-3′ (sense primer with a base substitution at t) and

5′-TTTCCCATCCaGGTCACAGCCTTCA-3′ (antisense primer with a base substitution at a).

We transfected human embryonic kidney cells (HEK293) with the prothrombin expression vectors using the calcium phosphate method.[8] We established stable transformants by selection with G418 and determined which of these had high levels of prothrombin expression by means of a dot-blot immunoassay. Conditioned media of stable transformants expressing recombinant prothrombins in serum-free medium containing vitamin K were collected, concentrated, and stored at −80°C until use. We determined the antigen levels of the prothrombins using an enzyme-linked immunosorbent assay (ELISA, Enzyme Research Laboratories).

FUNCTIONAL ASSAYS OF RECOMBINANT PROTHROMBINS

We performed three tests of prothrombin activity: a one-stage clotting assay, a two-stage clotting assay, and a chromogenic assay that uses S-2238 (a thrombin substrate that generates color at the time of cleavage). In the latter two assays, we used *Oxyuranus scutellatus* venom (Sigma Aldrich) as a factor Xa–like enzyme. To examine the functions of the recombinant prothrombins in plasma, we prepared reconstituted plasma by mixing prothrombin-deficient plasma (prothrombin activity, <1%; Mitsubishi Chemical Medience) with the recombinant prothrombins on the assumption that the prothrombin concentration was 100 μg per milliliter in normal plasma (100%).[9] The proband's plasma was not suitable for evaluation because of warfarin treatment.

FORMATION OF THROMBIN–ANTITHROMBIN COMPLEX

To evaluate the ability of the wild-type and mutant recombinant prothrombins to form complexes with antithrombin, we converted the recombinant prothrombins to thrombins, using bovine factors Xa (Haematologic Technologies) and Va (Thermo Scientific), cephalin (Roche Diagnostica Stago), and calcium chloride. We then incubated the thrombins with human antithrombin (Mitsubishi Tanabe Pharma), with or without unfractionated heparin (Mochida Pharmaceutical), at 37°C for various time periods. The reactions were stopped with PPACK (D-phenylalanyl-L-prolyl-L-arginine chloromethyl ketone) (Calbiochem), and thrombin–antithrombin complex formation was measured with the use of the AssayMax Human TAT Complexes ELISA kit (Assaypro).

THROMBIN-GENERATION ASSAY

We prepared wild-type, mutant, and heterozygous-mutant reconstituted plasma by mixing prothrombin-deficient plasma with the recombinant prothrombins, at a final prothrombin concentration of 100%, and by mixing antithrombin-depleted plasma (Affinity Biologicals) with human antithrombin, at a final antithrombin concentration of 50%. We used normal pooled plasma as a control. The thrombin-generation assay was performed by means of calibrated automated thrombography (CAT, Thrombinoscope BV), in accordance with the manufacturer's instructions. We monitored the reactions for 2 hours, using Fluoroscan Ascent FL (Thermo LabSystems), set at an excitation wavelength of 390 nm and an emission wavelength of 460 nm, and Thrombinoscope software (Thrombinoscope BV).

STUDY OVERSIGHT

The study was approved by the ethics committee at the Nagoya University School of Medicine. Written informed consent was obtained from all study participants.

RESULTS

DNA ANALYSIS

Genomic DNA analysis of the proband revealed that she was heterozygous for a novel missense mutation in the prothrombin gene (c.1787G→T, p.Arg596Leu) (Fig. 1B). The nucleotide and protein numbering system is based on the nomenclature recommended by the Human Genome Variation Society.[10] The same mutation was detected in her mother and in three other family members with deep-vein thrombosis but not in an asymptomatic family member. On mismatch PCR-RFLP analysis, the amplicon that was treated with PstI displayed a 192-bp band (mutant allele) and a 212-bp band (normal allele). We confirmed the heterozygosity of this mutation in the proband, her mother, and three other family members with deep-vein thrombosis but not in an asymptomatic family member (Fig. 1C). We did not detect the mutation in samples obtained from 100 Japanese persons with a normal phenotype and in 5 persons with undiagnosed thrombosis before this testing.

RECOMBINANT PROTHROMBINS

We established stable transformants of HEK293 cells expressing the wild-type and mutant prothrombins. To evaluate γ-carboxylation of the recombinant prothrombins, we used ELISA to measure prothrombin levels in the culture medium after barium sulfate absorption. We found that both the wild-type and mutant prothrombins were completely absorbed, suggesting that appropriate γ-carboxylation occurred in both preparations (data not shown).

FUNCTIONAL ASSAYS OF RECOMBINANT PROTHROMBINS

We performed three assessments of recombinant prothrombin activity: one-stage clotting, two-stage clotting, and chromogenic assays (Table 1). Reconstituted plasma was used in all tests. Values for the wild-type recombinant prothrombin were approximately 100% in all assays. The mutant prothrombin activity in the one-stage assay was lower than that in the two-stage assay. The mutant prothrombin activity in the chromogenic assay was higher than that in the two-stage assay.

FORMATION OF THROMBIN–ANTITHROMBIN COMPLEX

We used ELISA to determine whether there was a difference between the wild-type and mutant prothrombins in forming thrombin–antithrombin complexes. The recombinant prothrombins that were activated by factor Xa were incubated with antithrombin, and thrombin–antithrombin complex formation was determined by means of ELISA. In the absence of heparin, thrombin–antithrombin complex formation by the wild-type prothrombin increased in a time-dependent manner. However, thrombin–antithrombin complex formation by the mutant prothrombin was almost negligible for the first 30 minutes (Fig. 1D). In the presence of heparin, thrombin–antithrombin complex formation was greatly increased in both samples but remained substantially impaired in the mutant sample.

THROMBIN-GENERATION ASSAY

A thrombin-generation assay was performed to evaluate the effect of the mutation on thrombin generation in plasma (Fig. 2). The values for wild-type reconstituted plasma were similar to those for normal plasma, but the mutant plasma showed a decreased maximum concentration of thrombin (peak), an extension of the total duration of thrombin-generation activity (start tail), and increased thrombin activity, which was assessed as the area under the curve for endogenous thrombin potential. The heterozygous-mutant plasma, mimicking the proband's plasma, showed intermediate values. The 50% antithrombin plasma, mimicking the antithrombin-deficient plasma, showed similar changes (except for a decreased peak), which were canceled by the addition of human antithrombin at a final concentration of 150%. These data indicate that the thrombin activity derived from the mutant prothrombin was lower than that derived from the wild-type prothrombin, but its inactivation was exceedingly slow, resulting in a prolonged procoagulant state in the proband's plasma.

Table 1. Procoagulant and Amidolytic Activities of the Recombinant Prothrombins.*

Prothrombin	Antigen†	Activity‡		
		One-Stage Clotting Assay	Two-Stage Clotting Assay	Chromogenic Assay
		percent		
Wild-type	112	91	109	88
Mutant	118	15	32	66

* The values were measured in reconstituted prothrombin-deficient plasma. The value of normal plasma was assigned as 100%.
† The values for prothrombin antigens were determined by means of enzyme-linked immunosorbent assay.
‡ The prothrombin activities were determined by three methods: the classic one-stage clotting assay, in which thromboplastin is used; the two-stage clotting assay, in which *Oxyuranus scutellatus* venom (Ox) is used as a factor Xa–like enzyme and fibrinogen from pooled normal plasma is used as a substrate; and the chromogenic assay, in which Ox venom is used as an activator and S-2238 as a substrate.

DISCUSSION

Numerous gene mutations in various molecules have been found in members of families with inherited thrombophilia, but many mutations remain unidentified.[3] The G20210A mutation in the prothrombin gene is associated with a mild risk of thrombosis in the white population, but many other prothrombin gene mutations lead to bleeding tendencies, such as prothrombin deficiencies, dysprothrombinemia, and hypoprothrombinemia.[11-13] A genomewide analysis to detect genes that are associated with a susceptibility to thrombosis also identified a prothrombin gene mutation, but the detailed molecular mechanism for

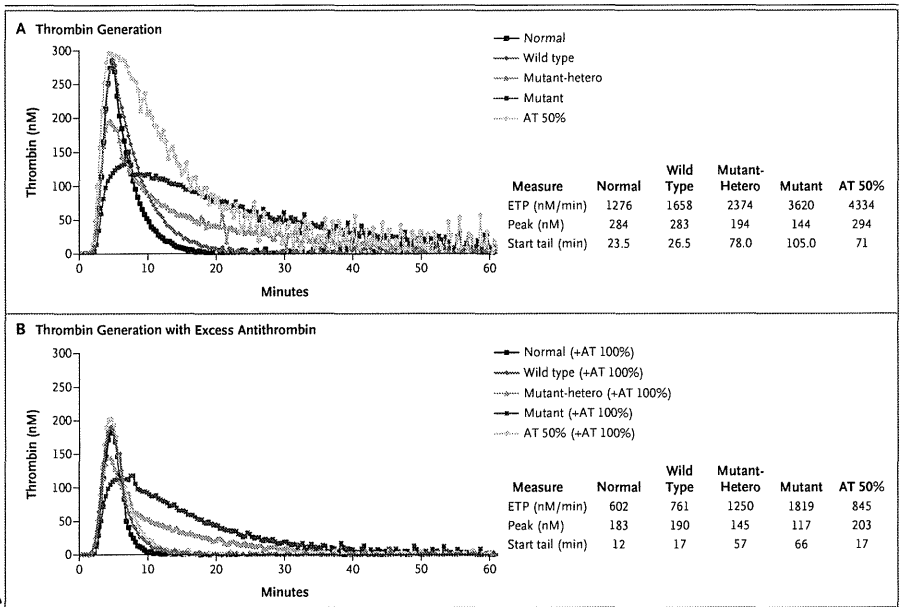

Measure	Normal	Wild Type	Mutant-Hetero	Mutant	AT 50%
ETP (nM/min)	1276	1658	2374	3620	4334
Peak (nM)	284	283	194	144	294
Start tail (min)	23.5	26.5	78.0	105.0	71

Measure	Normal	Wild Type	Mutant-Hetero	Mutant	AT 50%
ETP (nM/min)	602	761	1250	1819	845
Peak (nM)	183	190	145	117	203
Start tail (min)	12	17	57	66	17

Figure 2. Thrombin-Generation Assays with and without Excess Antithrombin.

Panel A shows the results of a thrombin-generation assay of normal plasma as well as reconstituted plasma samples, with recombinant prothrombins in prothrombin-deficient plasma and of human antithrombin (AT 50%) in antithrombin-depleted plasma. The heterozygous-mutant (mutant-hetero) plasma contained 50% each of wild-type and mutant prothrombin. The table at the right shows the total amount of thrombin activity, which was assessed as the area under the curve for endogenous thrombin potential (ETP), the maximum concentration of thrombin (peak), and the total duration of thrombin-generation activity (start tail). Panel B shows the results of a thrombin-generation assay of the respective plasma samples after the addition of excess antithrombin.

inherited thrombophilia remains unknown.[14] In this study, we investigated possible causative genetic defects in samples obtained from a large Japanese family with inherited thrombophilia. We found a novel missense mutation in the prothrombin gene (p.Arg596Leu) that resulted in a variant prothrombin (prothrombin Yukuhashi). The mutation cosegregated with deep-vein thrombosis in this family, indicating that it could be a cause of hereditary thrombophilia.

Thrombin, which is an active form of prothrombin, is an allosteric enzyme controlled by the binding of sodium.[15,16] Sodium-bound thrombin (known as the fast form) is optimized for procoagulation because of its increased substrate specificity for fibrinogen, whereas sodium-free thrombin (known as the slow form) is an anticoagulant because of its increased specificity for cleaving protein C. The mutation occurred at residue Arg596 (Arg221a in the chymotrypsinogen numbering system[17]) within the sodium-binding region of thrombin and was expected to have an effect on sodium binding. The mutation is also located at one of the antithrombin-binding sites where thrombin is inactivated by antithrombin with heparin.[18] Two exosites on thrombin, the γ-loop and the sodium-binding region, are critical for stabilizing a thrombin–antithrombin complex[18] (Fig. S1A in the Supplementary Appendix). Two hydrogens of the Arg596 side chains of thrombin form hydrogen bonds with oxygen of the Asn265 side chain of antithrombin (Fig. S1B in the Supplementary Appendix). Therefore, we propose two hypotheses: first, that the procoagulant activity of the mutant prothrombin is somewhat impaired; and second, that complex formation involving the mutant thrombin and antithrombin is impaired, resulting in prolonged residual thrombin activity.

To test the first hypothesis, we examined the activation and procoagulant functions of the recombinant prothrombins. We prepared reconstituted plasma by mixing prothrombin-deficient plasma with the recombinant prothrombins, since the proband's plasma was not suitable for evaluation because of warfarin treatment. We observed that the mutant and wild-type prothrombins were fully converted to thrombins in a similar manner by prothrombinase within 5 minutes (Fig. S2 in the Supplementary Appendix). However, conversion of the mutant prothrombin to thrombin appeared to be a few seconds slower than that of the wild-type thrombin in the clotting assays. In addition, the mutant thrombin probably had a lower catalytic activity for fibrinogen than did the wild-type thrombin, which may have been the result of structural disruption of the sodium-binding region by the Leu596 substitution for Arg. In a previous study of alanine-scanning mutagenesis, thrombin with an Ala596 mutation showed a reduction by a factor of 5 in sodium-binding affinity, and its procoagulant activity was similar to that of the slow form of thrombin.[19] Similar mechanisms of structural disruption in the Leu596 mutant thrombin may have resulted in lower catalytic activity for fibrinogen.

To test the second hypothesis — that the mutant thrombin would be defective in terms of its interaction with antithrombin — we examined thrombin–antithrombin complex formation using ELISA. The mutant thrombin sample had extremely low levels of thrombin–antithrombin complex formation. This suggests that the disruption of the sodium-binding region, which resulted in the loss of two hydrogen bonds between Arg596 of thrombin and Asn265 of antithrombin, may be critical for the formation of the thrombin–antithrombin complex. These findings indicate that prothrombin Yukuhashi can be characterized as a dysprothrombin that is highly resistant to inhibition by antithrombin.

We next performed a thrombin-generation assay to determine the potential procoagulant activity of the recombinant prothrombins in plasma. A thrombin-generation assay is a comprehensive coagulation-function test that allows evaluation not only of the initial phase of thrombin generation but also of the late phase of its inactivation. Data from this assay again suggested that the mutant prothrombin had low procoagulant activity but was highly resistant to antithrombin. Thus, its active form, the mutant thrombin, would not be inactivated by antithrombin and would continue to facilitate blood coagulation, despite its low activity level.

In conclusion, we identified a novel mechanism of hereditary thrombosis in a Japanese family, in which antithrombin resistance was associated with a missense mutation in the prothrombin gene (p.Arg596Leu). This mutation results in slightly impaired but adequate procoagulant function of the mutant prothrombin but considerably impaired inhibition of the mutant thrombin by antithrombin. The antithrombin-resistant thrombin may have prolonged procoagulant activity in vivo, conferring a susceptibility to thrombosis.

Supported in part by grants from the Japanese Ministry of Education, Culture, Sports, Science, and Technology; the Japanese Ministry of Health, Labor and Welfare; and the Senshin Medical Research Foundation.

Disclosure forms provided by the authors are available with the full text of this article at NEJM.org.

We thank C. Wakamatsu for providing technical assistance, and Enago for translation services.

REFERENCES

1. De Stefano V, Finazzi G, Mannucci P. Inherited thrombophilia: pathogenesis, clinical syndromes, and management. Blood 1996;87:3531-44.
2. Rosendaal FR. Venous thrombosis: a multicausal disease. Lancet 1999;353:1167-73.
3. Khan S, Dickerman JD. Hereditary thrombophilia. Thromb J 2006;4:15.
4. Sakai M, Urano H, Iinuma A, Okamoto K, Ohsato K, Shirahata A. A family with multiple thrombosis including infancy occurrence. J UOEH 2001;23:297-305. (In Japanese.)
5. Okada H, Takagi A, Murate T, et al. Identification of protein S alpha gene mutations including four novel mutations in eight unrelated patients with protein S deficiency. Br J Haematol 2004;126:219-25.
6. Kojima T, Tanimoto M, Kamiya T, et al. Possible absence of common polymorphisms in coagulation factor IX gene in Japanese subjects. Blood 1987;69:349-52.
7. Suzuki A, Nakashima D, Miyawaki Y, et al. A novel ENG mutation causing impaired co-translational processing of endoglin associated with hereditary hemorrhagic telangiectasia. Thromb Res 2012;129(5):e200-e208.
8. Suzuki A, Sanda N, Miyawaki Y, et al. Down-regulation of PROS1 gene expression by 17β-estradiol via estrogen receptor α (ERα)-Sp1 interaction recruiting receptor-interacting protein 140 and the corepressor-HDAC3 complex. J Biol Chem 2010;285:13444-53.

9. Lundblad RL, Kingdon HS, Mann KG. Thrombin. Methods Enzymol 1976;45:156-76.
10. den Dunnen JT, Antonarakis SE. Mutation nomenclature extensions and suggestions to describe complex mutations: a discussion. Hum Mutat 2000;15:7-12. [Erratum, Hum Mutat 2002;20:403.]
11. Akhavan S, Mannucci P, Lak M, et al. Identification and three-dimensional structural analysis of nine novel mutations in patients with prothrombin deficiency. Thromb Haemost 2000;84:989-97.
12. Lefkowitz JB, Weller A, Nuss R, Santiago-Borrero PJ, Brown DL, Ortiz IR. A common mutation, Arg457→Gln, links prothrombin deficiencies in the Puerto Rican population. J Thromb Haemost 2003;1:2381-8.
13. Poort SR, Rosendaal FR, Reitsma PH, Bertina RM. A common genetic variation in the 3′-untranslated region of the prothrombin gene is associated with elevated plasma prothrombin levels and an increase in venous thrombosis. Blood 1996;88:3698-703.
14. ten Kate M, He C, van Schouwenburg I, et al. A genome wide linkage scan for thrombosis susceptibility genes identifies a novel prothrombin mutation. Presented at the 22nd Congress of the International Society on Thrombosis and Haematosis, Boston, July 11–16, 2009. abstract.
15. Dang QD, Vindigni A, Di Cera E. An allosteric switch controls the procoagulant and anticoagulant activities of thrombin. Proc Natl Acad Sci U S A 1995;92:5977-81.
16. Pineda AO, Carrell CJ, Bush LA, et al. Molecular dissection of Na^+ binding to thrombin. J Biol Chem 2004;279:31842-53.
17. Bode W, Turk D, Karshikov A. The refined 1.9-Å X-ray crystal structure of d-Phe-Pro-Arg chloromethylketone-inhibited human α-thrombin: structure analysis, overall structure, electrostatic properties, detailed active-site geometry, and structure-function relationships. Protein Sci 1992;1:426-71.
18. Li W, Johnson DJD, Esmon CT, Huntington JA. Structure of the antithrombin-thrombin-heparin ternary complex reveals the antithrombotic mechanism of heparin. Nat Struct Mol Biol 2004;11:857-62.
19. Dang QD, Guinto ER, Cera ED. Rational engineering of activity and specificity in a serine protease. Nat Biotechnol 1997;15:146-9.

Supplementary data

Table of contents

Suppl. Methods

Conversion of recombinant prothrombins by the prothrombinase complex

Wild-type and mutant recombinant prothrombins (80 nM) were treated with a prothrombinase complex containing bovine factor Xa (10 nM; Haematologic Technologies), bovine factor Va (10 nM; Thermo Scientific), Cephalin (10% (v/v); PTT-reagent RD, Roche Diagnostica Stago) and 2 mM $CaCl_2$ in Tris-buffered saline and 0.01% (v/v) Tween-20 at 37°C. Reactions were initiated by the addition of factor Xa followed by the removal of aliquots at timed intervals. The samples were then separated by SDS-PAGE on 10% polyacrylamide gels under reducing conditions, and transferred to polyvinylidene difluoride membranes (Amersham Biosciences) for immunoblotting as described previously[1].

Suppl. Results

Conversion of the recombinant prothrombins by prothrombinase complex

Activation of prothrombin by the prothrombinase complex produced thrombin and varied derivatives[2]. The time courses of the activation patterns were similar in both recombinant prothrombins, as shown in Suppl. Fig. 1. Both prothrombin bands had almost disappeared after 5 min, demonstrating that the mutant prothrombin was proteolysed by the prothrombinase complex in a similar way to the wild-type prothrombin.

Suppl. Figure legends

Suppl. Fig. S1. Structural features of the thromin-antithrombin complex (PDB ID: 1TB6).

Panel A shows the crystal structure of the thrombin-antithrombin complex with heparin (left) and that of the hidden heparin (right). Thrombin (light blue, light chain; white, heavy chain) and antithrombin (green) are combined via two exosites with heparin (violet stick), the γ-loop binding region, and the Na^+ binding region (yellow circle). The blue residues are the active center of thrombin and the Arg596 of thrombin (arrowed yellow residue) is located away from the active center. The red residues of thrombin and the magenta residues of antithrombin are involved in thrombin-antithrombin complex formation.

Panel B shows Na^+ binding region interactions. The side chain of Arg596 (yellow) in thrombin forms two hydrogen bonds (light blue dashed line) with the side chain of Asn265 in antithrombin. Glu264 of antithrombin also forms a salt bridge with Lys599 of thrombin involving a water-mediated hydrogen bond network with surrounding residues Thr540, Arg541, Glu592 and Lys599[3]. Residues of thrombin and antithrombin are shown in white and green, respectively. The water molecule is shown as a light blue sphere.

Suppl. Fig. S2. Conversion of recombinant prothrombins by prothrombinase.

Recombinant wild-type and mutant prothrombins were activated at 37°C with 10 nM of bovine factors Xa and Va, 10% phospholipid in TBS, 2 mM $CaCl_2$, 0.01% (v/v) Tween-20, pH7.4. Aliquots of reaction mixtures were removed at the specified time intervals and analyzed by SDS-PAGE on 10% polyacrylamide gels before immunoblotting. The molecular weight markers are indicated on the left. The prothrombin fragments shown are as follows: FII, prothrombin; F1.2, fragment 1.2; P2, prothrombin-2; T_B, B chain of α-thrombin; and F1; fragment 1.

Suppl. Fig. S1. Structural features of the thrombin-antithrombin complex (PDB ID: 1TB6).

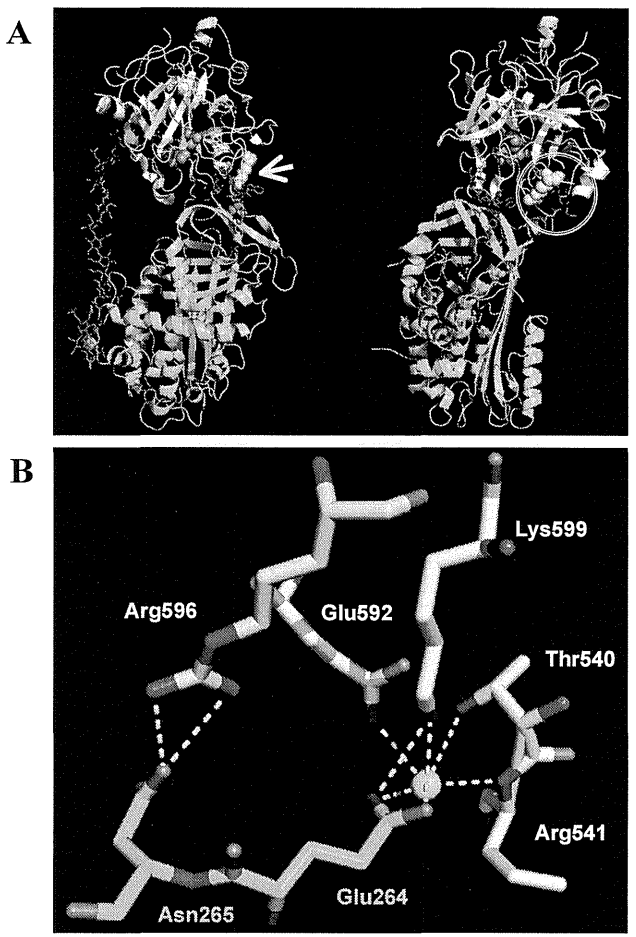

Suppl. Fig. S2. Activation of recombinant prothrombins by prothrombinase.

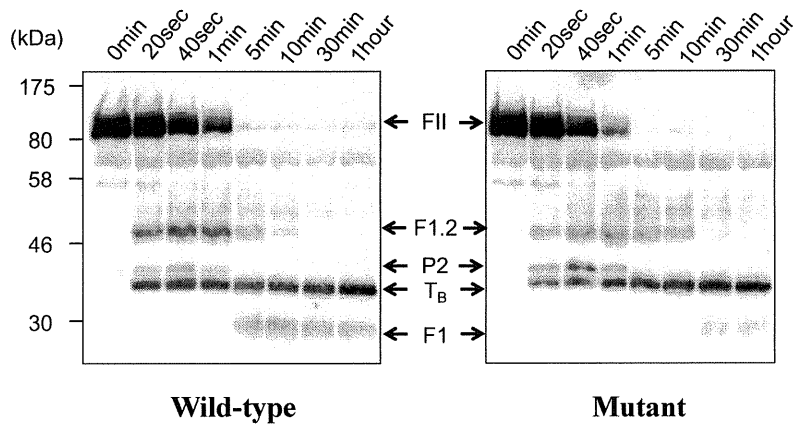

Suppl. Table S1. Primers for PCR amplification of the prothrombin gene.

exon		Oligonucleotide Sequence	Annealing (°C)	PCR product (bp)
1	Up	5'-TGGAGATGGACAGGAGGACT-3'	60	337
	Lw	5'-ACCTACTTAGGGGCCAGCTC-3'		
2	Up	5'-CCTCTCTCAGAAGCCAGCAG-3'	60	388
	Lw	5'-TGAAATGAGGCTGTGAGCAG-3'		
3–4	Up	5'-GCGTGACCAGGGTAAAGGAA-3'	60	493
	Lw	5'-AAACCCACCCCTGAGCTCTT-3'		
5–6	Up	5'-TGGGGGATAGACAACTTTGC-3'	60	499
	Lw	5'-TTCTTGGTTCCCATCCCAG-3'		
7	Up	5'-GTCACACAGGCAGAAAGCAG-3'	60	489
	Lw	5'-CAGAAGCGGCTGTTGTTATT-3'		
8–9	Up	5'-GATCTAGGGGATGGGTGAGG-3'	60	461
	Lw	5'-GGGTCCAGCAGCACACCT-3'		
10	Up	5'-GGGTTCTTAGACCTGGGATTG-3'	60	368
	Lw	5'-CATGATCGCTTTGGAGGACT-3'		
11	Up	5'-GCAGGACACACTGTCTCCCAGAC-3'	60	368
	Lw	5'-AAAAGGGAAAGGGGCTCTTGC-3'		
12	Up	5'-CCAGCTCTGGCGTTTTAGAT-3'	60	400
	Lw	5'-TGAGCCACCAAGAGGTTAGG-3'		
13	Up	5'-AAGTGGGGACAGCAAGAATGA-3'	60	309
	Lw	5'-GAGTCAAGTTCAAGGTCACATCAG-3'		
14	Up	5'-AGGGCCTGGTGAACACATCTTC-3'	60	467
	Lw	5'-CCAGGTGGTGGATTCTTAAGTCTTC-3'		

Suppl. References

1. Suzuki A, Sanda N, Miyawaki Y, et al. Down-regulation of PROS1 Gene Expression by 17beta-Estradiol via Estrogen Receptoralpha (ERalpha)-Sp1 Interaction Recruiting Receptor-interacting Protein 140 and the Corepressor-HDAC3 Complex. J Biol Chem 2010;285:13444-53.
2. Chen Z, Pelc LA, Di Cera E. Crystal structure of prethrombin-1. Proc Natl Acad Sci 2010;107:19278-83.
3. Li W, Johnson DJD, Esmon CT, Huntington JA. Structure of the antithrombin-thrombin-heparin ternary complex reveals the antithrombotic mechanism of heparin. Nat Struct Mol Biol 2004;11:857-62.